J Neuropathol Exp Neurol
Vol. 74, No. 7
July 2015
pp. 653–671

ORIGINAL ARTICLE

Cell Junction Pathology of Neural Stem Cells Is Associated With Ventricular Zone Disruption, Hydrocephalus, and Abnormal Neurogenesis

María Montserrat Guerra, PhD, Roberto Henzi, PhD, Alexander Ortloff, PhD, Nicole Lichtin, PhD, Karin Vío, PhD, Antonio J. Jiménez, PhD, María Dolores Dominguez-Pinos, MD, César González, PhD, Maria Clara Jara, Fernando Hinostroza, PhD, Sara Rodríguez, PhD, Maryoris Jara, MSc, Eduardo Ortega, MD, Francisco Guerra, MD, Deborah A. Sival, MD, Wilfred F. A. den Dunnen, MD, José M. Pérez-Fígares, PhD, James P. McAllister, PhD, Conrad E. Johanson, PhD, and Esteban M. Rodríguez, MD, PhD

Abstract

Fetal-onset hydrocephalus affects 1 to 3 per 1,000 live births. It is not only a disorder of cerebrospinal fluid dynamics but also a brain disorder that corrective surgery does not ameliorate. We hypothesized that cell junction abnormalities of neural stem cells (NSCs) lead to the inseparable phenomena of fetal-onset hydrocephalus and abnormal neurogenesis. We used bromodeoxyuridine labeling, immunocytochemistry, electron microscopy, and cell culture to study the telencephalon of hydrocephalic HTx rats and correlated our findings with those in human hydrocephalic and nonhydrocephalic human fetal brains (n = 12 each). Our results suggest that abnormal expression of the intercellular junction proteins N-cadherin and connexin-43 in NSC leads to 1) disruption of the ventricular and subventricular zones, loss of NSCs and neural progenitor cells; and 2) abnormalities in neurogenesis such as periventricular heterotopias and abnormal neuroblast migration. In HTx rats, the disrupted NSC and progenitor cells are shed into the cerebrospinal fluid and can be grown into neurospheres that display intercellular junction abnormalities similar to those of NSC of the disrupted ventricular zone; nevertheless, they maintain their potential for differentiating into neurons and glia. These NSCs can be used to investigate cellular and molecular mechanisms underlying this condition, thereby opening the avenue for stem cell therapy.

Key Words: Cerebrospinal fluid, Congenital hydrocephalus, HTx rat, Human, Junction pathology, Neural stem cells, Neurospheres, Ventricular zone disruption.

INTRODUCTION

Fetal-onset hydrocephalus is heterogeneous. Genetic mutations, such as X-linked hydrocephalus (1), distal neural tube defects, namely, spina bifida (2), and environmental factors, such as nutritional deficiencies (3), viral infection of ependyma (4), and prematurity-related intraventricular hemorrhage (5), contribute to its occurrence. Congenital hydrocephalus affects 1 to 3 of 1,000 live births and is characterized by abnormal cerebrospinal fluid (CSF) flow that results in ventricular dilatation (6). Surgical diversion of CSF (shunting) does not resolve most aspects of this disease (7). Indeed, 80% to 90% of the neurologic impairments suffered by shunt-dependent neonates with fetal-onset hydrocephalus are not reversed by surgery. How then can we explain the inborn and, so far, irreparable neurologic impairment of children born with hydrocephalus? Recent studies have begun to identify cellular pathogenesis that accompanies fetal-onset hydrocephalus (2, 8–11), but the nature, mechanism, and extent of the brain impairment linked to congenital hydrocephalus are not understood.

Most cells of the developing mammalian brain derive from the ventricular zone (VZ) and subventricular zone (SVZ), which are formed by the radial glia/neural stem cells (NSCs) and neural progenitor cells (NPCs), respectively (12–14). A large body of evidence obtained from several mutant animals and some human cases of fetal-onset hydrocephalus indicates that the disruption of the VZ of the cerebral aqueduct is associated with the onset of hydrocephalus (15–19). The disruption process starts early in fetal life and finishes during the first postnatal weeks, affecting equally the NSCs and the ependymal cells forming the VZ at prenatal and postnatal stages of development (9, 16–19).

From the Instituto de Anatomía, Histología y Patología (MMG, RH, AO, NL, KV, CG, MCJ, FH, SR, MJ, EMR), Instituto de Neurociencias Clínicas (EO), Instituto de Obstetricia y Ginecología (FG), Universidad Austral de Chile, Valdivia, Chile; Facultad de Recursos Naturales (AO), Escuela de Medicina Veterinaria, Universidad Católica de Temuco, Araucania, Chile; Departments of Pediatric Neurology and Pediatrics (DAS), and Pathology and Medical Biology (WFAdD), University Medical Center, University of Groningen, Groningen, The Netherlands; Departamento de Biología Celular, Facultad de Ciencias, Universidad de Málaga, Málaga, Spain (AJJ, MDD-P, JMP-F); Department of Neurosurgery, Pediatric Neurosurgery Division, University of Utah, Salt Lake City, Utah (JPMA); and Department of Neurosurgery, Alpert Medical School at Brown University, Providence, Rhode Island (CEJ).

María Montserrat Guerra and Roberto Henzi contributed equally to this work.

Send correspondence and reprint requests to: María Montserrat Guerra, PhD, Instituto de Anatomía, Histología y Patología, Facultad de Medicina, Universidad Austral de Chile, Valdivia, Chile; E-mail: monserratguerra@uach.cl

This work was supported by Fondecyt (Chile) grants 1070241 and 1111018 to Esteban M. Rodriguez; Hydrocephalus Association Established Investigator Award (No. 51002705) to James P. McAllister, Esteban M. Rodriguez, and Conrad E. Johanson; Instituto de Salud Carlos III (Spain) grants PI12/0631 and FEDER and Ministerio de Educación y Ciencia (Spain) (PCI2006-A/-0669) to Antonio J. Jiménez; and Universidad Austral de Chile/DID S-2006-72 to Karin Vío.

Although a disrupted VZ occurs in the telencephalon of hydrocephalic patients and mutant rodents (11, 17, 20), little is known about the mechanism of disruption and the outcomes. There is evidence that abnormalities of cell junctions involving adherent and gap junctions are implicated in VZ disruption (9, 16, 20–22). However, there are few reports on the role of adherent and gap junctions in the pathophysiology of abnormal neurogenesis in fetal-onset hydrocephalus (20, 23). We hypothesized that cell junction pathology of NSCs, involving abnormal expression of N-cadherin and connexin-43, leads to both hydrocephalus and abnormal neurogenesis. To test this hypothesis, we analyzed mutant HTx rats, which develop fetal-onset noncommunicating hydrocephalus, as well as human cases of fetal-onset hydrocephalus. The evidence obtained uniformly supports the hypothesis that a dislodging of intercellular N-cadherin and connexin-43 in NSCs is associated with VZ/SVZ disruption, formation of periventricular heterotopias (PHs), and displacement of NSCs into the CSF. Neurospheres experimentally formed from the displaced cells have characteristics similar to the disrupted zones in vivo and, therefore, may prove useful in further molecular analyses of congenital disorders such as PH and hydrocephalus.

MATERIALS AND METHODS

Human Brain Specimens

This study was performed on fetal specimens obtained from the University Hospital, Groningen, The Netherlands; the Pathology Department of Carlos Haya Hospital, Málaga, Spain; and the Regional Hospital of Valdivia, Chile. The medical ethics committees of the 3 hospitals approved the study. The respective families had given informed consent. Twelve hydrocephalic and 12 control human fetuses, ranging between 16 and 40 gestational weeks (GWs), were investigated (Table). Histologic sections of the brainstem (cerebral aqueduct) of Cases 1 to 5 (Table) were used in a previous study (16). Cases 2 to 5 displayed major abnormalities compromising life expectancy; these included progressively devastating hydrocephalus with signs of incarceration (hampering delivery requiring cephalocentesis) and underdevelopment of lungs and heart. Control cases had no neuropathologic alterations. Four to 6 tissue blocks were obtained from each brain; they were serially cut, producing a series of several hundreds of 5-μm-thick sections. For each series, every 20th section was mounted side by side, obtaining 20 semiseries per tissue block that were used for hematoxylin and eosin stain, immunocytochemistry, and double immunofluorescence analyses.

Animals

Rats of the HTx strain (7) were obtained from the laboratory of Dr Hazel Jones (University of Florida, Gainesville, FL) in 2002 and bred into a colony in the Animal Facility at the Instituto de Anatomía Histología y Patología, Universidad Austral de Chile, Valdivia, Chile. Housing, handling, care, and processing of animals were carried out according to regulations approved by the National Research Council of Chile (Conicyt). The ethics committees of Universidad Austral de Chile and the University of Utah approved the experimental

TABLE. Hydrocephalic and Control Human Fetuses

Case No./Diagnosis	Gestational Age, weeks	Delivery	Source	Fixation
1. SBA	21	Abruptio placentae	G	4% PF in PBS pH 7.4
2. SBA	22	Induced by PGE2	G	4% PF in PBS pH 7.4
3. SBA	37	Induced by PGE2	G	4% PF in PBS pH 7.4
4. SBA	39	Induced by PGE2	G	4% PF in PBS pH 7.4
5. SBA	40	Induced by PGE2	G	4% PF in PBS pH 7.4
6. Hy	30	Spontaneous abortion	M	5% formalin
7. Hy	31	Spontaneous abortion	M	5% formalin
8. Hy	34	Spontaneous abortion	M	5% formalin
9. SBA	20	Spontaneous abortion	M	5% formalin
10. SBA	22	Spontaneous abortion	M	5% formalin
11. SBA	36	Spontaneous abortion	M	5% formalin
12. Hy, Potter syndrome	40	Spontaneous abortion	M	5% formalin/Bouin
13. Control	22	Premature labor	G	4% PF in PBS pH 7.4
14. Control	33	Premature labor	G	4% PF in PBS pH 7.4
15. Control	37	Twin pregnancy cesarean section	G	4% PF in PBS pH 7.4
16. Control	41	Umbilical cord strangulation	G	4% PF in PBS pH 7.4
17. Control	16	Spontaneous abortion	M	5% formalin
18. Control	21	Spontaneous abortion	M	5% formalin
19. Control	30	Spontaneous abortion	M	5% formalin
20. Control	22	Spontaneous abortion	M	5% formalin
21. Control, Potter syndrome	21	Spontaneous abortion	M	5% formalin
22. Control	16	Spontaneous abortion	V	5% formalin
23. Control	21	Spontaneous abortion	V	5% formalin
24. Control	22	Spontaneous abortion	V	5% formalin

G, Groningen; Hy, isolated hydrocephalus; M, Málaga; PBS, phosphate buffered saline; PF, paraformaldehyde; PGE2, prostaglandin E2; SBA, spina bifida aperta; V, Valdivia.

protocol. The hydrocephalic phenotype was identified from an overtly domed head and by transillumination of the head of newborns. Definitive diagnosis was made by microscopic analysis of the brain, particularly the subcommissural organ, because, from E15 onward, the hydrocephalic HTx rats display a specific development defect in the subcommissural organ (24).

Tissue Processing for Light Microscopy

The following nonhydrocephalic (nHTx) and hydrocephalic (hyHTx) HTx rats were processed for immunocytochemistry: 1) Fetal Day 18 (E18, n = 7 nHTx, 8 hyHTx), E19 (n = 2 nHTx, 2 hyHTx), E20 (n = 5 nHTx, 5 hyHTx); Postnatal Day 1 (PN1, n = 6 nHTx, 10 hyHTx), PN5 (n = 3 nHTx, 4 hyHTx), PN7 (n = 4 nHTx, 4 hyHTx), PN21 (n = 6 nHTx, 6 hyHTx). Pregnant and newborn rats were anesthetized with ketamine (40 mg/kg) and acepromazine (100 mg/kg). Fetuses were dissected from the uterus, the head was removed, and a sagittal cut through the lateral region of the skull was performed to expose the lateral ventricle and the subarachnoid space to the fixative. Postnatally, brains were fixed by intravascular perfusion with Bouin fixative. The brains were then processed and embedded in paraffin. The telencephalon of each rat was cut serially at a thickness of 5 μm. Every 10th section of the series was mounted side by side, obtaining 10 semiseries of sections that were used for immunocytochemistry and immunofluorescence. In addition, the brains of 4 PN7 hyHTx rats were fixed by immersion in 4% paraformaldehyde, and the roof of the lateral ventricles was processed for whole-mount double immunofluorescence for N-cadherin/βIV-tubulin and connexin-43/βIV-tubulin.

Immunohistochemistry

Sections from human and HTx rat brains, and from neurospheres (see below), were processed for immunohistochemistry as described by Sternberger et al (25) or the streptavidin-biotin method (Vectastain kit; Vector, Serva, Heidelberg, Germany), with diaminobenzidine as chromogen. Antibodies against the following compounds were used: βIV-tubulin, monoclonal (Abcam, Cambridge, UK); CD99, monoclonal (Dako, Glostrup, Denmark); glial fibrillary acidic protein (GFAP), raised in rabbit (Sigma, St. Louis, MO); βIII-tubulin, monoclonal (Sigma); nestin, monoclonal (Developmental Studies Hybridoma Bank, Iowa City, IA); caveolin 1 (Santa Cruz Biotechnology, Inc, Santa Cruz, CA); N-cadherin raised in rabbit (Santa Cruz Biotechnology, Inc); pan-cadherin (recognize all the types of cadherins; Sigma); connexin-43, raised in rabbit (gift from Dr Juan Carlos Sáez, Universidad Católica de Chile, Santiago, CL); bromodeoxyuridine (BrdU), monoclonal (Developmental Studies Hybridoma Bank). Antibodies were diluted in a buffer containing 0.1 mol/L Tris buffer, pH 7.8, 0.7% nongelling seaweed gelatin, lambda carrageenan, and 0.5% Triton X-100 (Sigma). Incubation was carried out for 18 hours at room temperature. Omission of the primary antibody during incubation provided the control for the immunoreactions.

Double Immunofluorescence and Confocal Microscopy

Sections from neurospheres and human and HTx rat brains were processed for double immunofluorescence using the following pairs of antibodies: anti-nestin/anti–caveolin 1; anti–caveolin 1/anti–βIV-tubulin; anti–N-cadherin/anti–βIV-tubulin; anti–βIV-tubulin/anti–connexin-43; anti-GFAP/anti–βIII-tubulin; anti-nestin/anti–caveolin 1; anti-BrdU/anti–βIII-tubulin; anti-BrdU/anti-GFAP; and anti-BrdU/anti–βIV-tubulin. Appropriate secondary antibodies conjugated with Alexa Fluor 488 or 594 (1:500; Invitrogen, Carlsbad, CA) were used. Slides were studied under an epifluorescence microscope using the multidimensional acquisition software AxioVision Rel (version 4.6) of Zeiss (Aalen, Germany) or a confocal microscope (Leica SP5 II) or by spectral confocal microscopy (Zeiss LSM780) with the 3D acquisition software Zen 2011, V8.0.

BrdU Labeling and Immunocytochemistry of CSF Cells

Postnatal Day 5 hyHTx rats (n = 4) were injected 3 times, at 1-hour intervals, with BrdU (Sigma; 100 mg/kg body weight) and killed 1 hour after the last injection. Brains were fixed by vascular perfusion with Bouin fixative. Tissue sections were processed for immunohistochemistry with anti-BrdU. The same BrdU protocol was applied to PN1 hyHTx rats (n = 4); 1 hour after the last injection, CSF samples from a lateral ventricle were centrifuged at 1,000 × *g* for 1 minute. The resulting cell pellets were fixed in Bouin fluid and embedded in paraffin. Five-micrometer-thick sections were processed for anti-BrdU, anti–βIII-tubulin, and anti-nestin immunocytochemistry.

BrdU Labeling and Immunocytochemistry of PH

Postnatal Day 7 (n = 6), PN21 (n = 6), and PN30 (n = 4) hyHTx rats were injected 3 times, at 1-hour intervals, with BrdU (Sigma; 100 mg/kg body weight) and killed 1 hour after the last injection. Brains were fixed by vascular perfusion with Bouin fixative. Tissue sections were processed for immunohistochemistry and double immunofluorescence using anti-BrdU and others antibodies.

Neurospheres From Brain Tissue

Postnatal Day 1 nHTx rats anesthetized with ketamine (40 mg/kg) and acepromazine (100 mg/kg) were killed by decapitation. The dorsolateral walls of both lateral ventricles containing the VZ/SVZ were excised under a microscope and placed in a 2-mL tube containing 1 mL of neurosphere culture medium (NeuroCult NS-A Proliferation Medium-Rat), supplemented with 20 ng/mL epidermal growth factor, and 2 μg/mL heparin (StemCell Technologies, Vancouver, CA) and 100 μg/mL penicillin/streptomycin (Sigma). The tissue was disaggregated mechanically and 1 mL of fresh culture medium was added. The cell suspension was centrifuged for 10 minutes at 110 × *g*; the resulting pellet was diluted (1:10) with culture medium and placed in a 12-well culture plate (TPP; Techno Plastic Products AG, Trasadingen, Switzerland). The cells were cultured for 6 days (DIV) and monitored by phase contrast microscopy; 10 μmol/L BrdU was added for the last 24 hours of culture. Neurospheres were collected and spun down, and the resulting pellet was fixed in Bouin fixative and embedded in paraffin. This procedure was carried out 30 times. The same protocol was used to study neurospheres obtained from the VZ/SVZ of PN1 hyHTx rats. This experiment was performed 5 times.

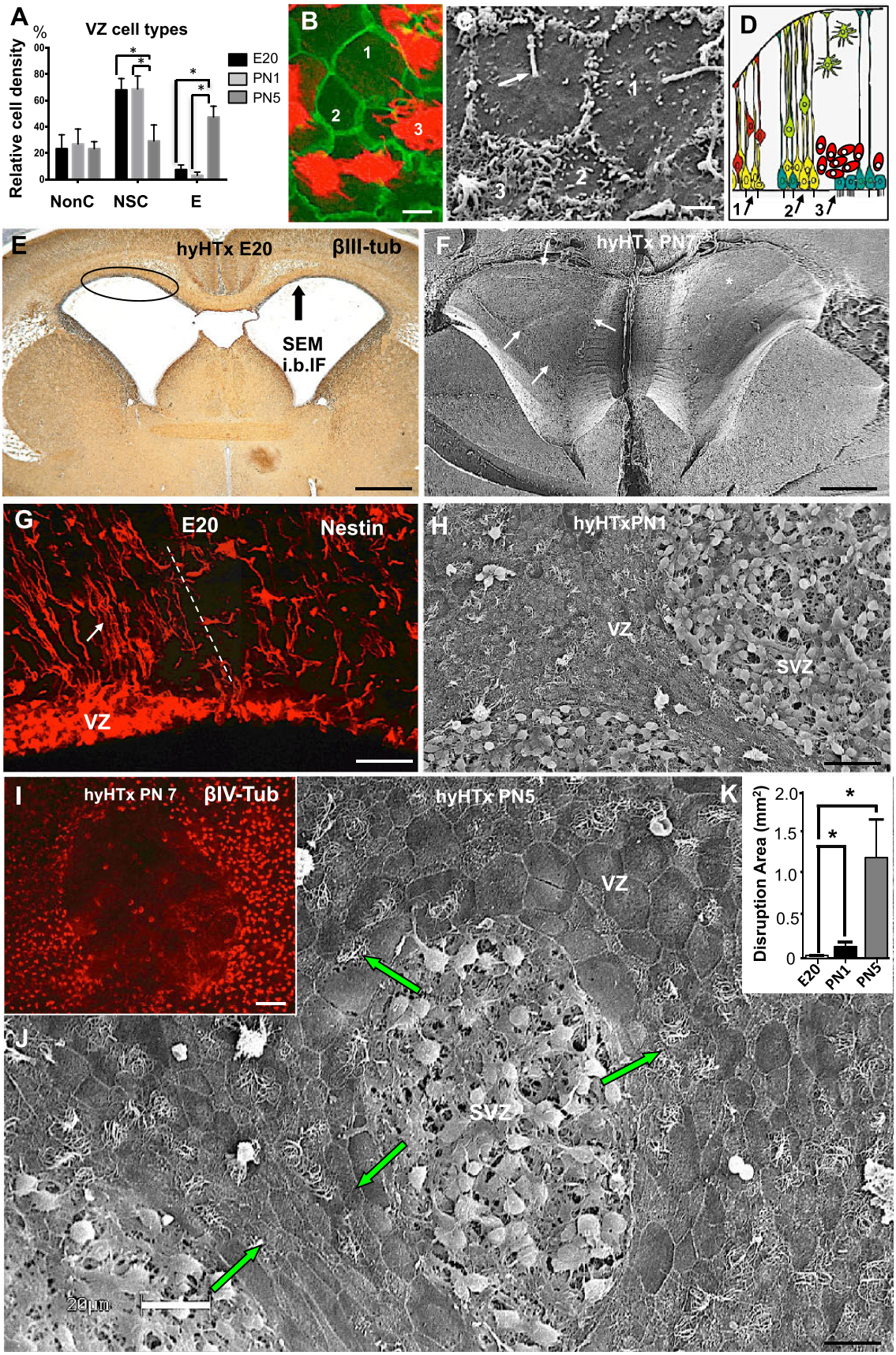

Neurospheres From CSF

Unaffected and hydrocephalic HTx PN1 rats were used for CSF collection. Pups were anesthetized with ketamine (40 mg/kg) and acepromazine (100 mg/kg). Cerebrospinal fluid was obtained from the cisterna magna (15 μL from each animal, nHTx) or from lateral ventricles (100 μL) of hyHTx rats. Cerebrospinal fluid samples from 5 to 7 animals were pooled, centrifuged at 1,000 × *g* for 30 seconds; the cells were then resuspended in culture medium and then plated in 1 well of a 12-well culture plate. The culture was maintained for 6 DIV and monitored by phase contrast microscopy; 10 μmol/L BrdU was added for the last 24 hours of culture. In some experiments, neurospheres were cultured for 7 days. Neurospheres were collected and spun down, and the pellet was fixed in Bouin fixative and embedded in paraffin. This experiment was performed 14 times for CSF from hydrocephalic rats (hyCSF) and 6 times for CSF of nonaffected animals. No neurospheres were obtained from the CSF collected via the cisterna magna of normal rats.

Differentiation Assay

After 6 DIV, neurospheres grown from VZ/SVZ of nHTx and hyHTx rats were collected and plated in differentiation medium (NeuroCult NS-A Differentiation Medium-Rat, StemCell Technologies) on a poly-ı-lysine–coated coverslip in a 12-well culture plate. The cultures were maintained for 2 to 3 weeks and monitored by microscopy. Cells were fixed with 4% paraformaldehyde and processed for double immunofluorescence analysis using anti–βIII-tubulin/anti-GFAP.

Transmission Electron Microscopy

Brains from E20 (n = 3 nHTx, 5 hyHTx), PN1 (n = 5 nHTx, 8 hyHTx), and PN3 (n = 4 nHTx, 5 hyHTx) rats were fixed for 2 hours in a fixative of 4% paraformaldehyde, 2% glutaraldehyde, and 2% acrolein in 0.2 mol/L phosphate buffer, pH 7.4 (26). A sagittal cut through the lateral region of the skull was made, and the fixative was gently subperfused into the exposed brain cavities. Blocks of tissue containing the roof of the lateral ventricles were postfixed in 1% OsO4 in 0.1 mol/L phosphate buffer, pH 7.4, for 2 hours at 4°C.

Scanning Electron Microscopy

Brains from nHTx (n = 8) and hyHTx (n = 20) rats (E20, PN1, PN3, PN5, PN7, PN10) were processed for scanning electron microscopy (SEM). Fixation was in 1% paraformaldehyde in 0.1 mol/L phosphate buffer, pH 7.4, for 2 hours. Tissue blocks were critical point dried, whereas neurospheres were dehydrated by a series of alcohols and acetone.

Data Analysis

Seventy-two electron micrographs obtained with the scanning electron microscope were used for image analyses to quantify the 1) area size of disrupted VZ of the telencephalon at E20, PN1, PN5 manually traced with NIH ImageJ and tabulated. Normality of data distribution was tested with D'Agostino-Pearson omnibus test. Data were expressed as average ± SE with $p \leq 0.05$. 2) The relative cell density of NSCs, ependymal cells, and nonciliated cells of the pallium of E20, PN1, and PN5. Ordinary one-way analysis of variance with a Bonferroni multiple comparison test was applied. Data were expressed as average ± SE with $p \leq 0.05$. Statistical analysis of data was made using Prism GraphPad 6.0 (GraphPad Software, Inc, San Diego, CA).

RESULTS

There is evidence that VZ disruption at the cerebral aqueduct is associated with the onset of hydrocephalus (16–19). The following findings obtained in the HTx rat model and in humans developing fetal-onset hydrocephalus suggest that the process of VZ disruption also reaches the telencephalon, resulting in abnormalities of neurogenesis.

The VZ of the HTx Telencephalon Displays a Temporospatial Pattern of Differentiation

There were distinct developmental differences between the medial and the laterodorsal walls of the lateral ventricles of HTx. Thus, from E20 onward, the VZ of the medial wall was formed by multiciliated ependymal cells whereas the VZ of the lateral and dorsal walls was formed by 3 cell types readily visualized with SEM and immunocytochemistry: 1) NSCs that were nestin positive and displayed a single cilium (Fig. 1B, C, D, G); 2) nonciliated cells that were distinguishable in whole-mount immunostaining for βIV-tubulin and N-cadherin and with SEM (Fig. 1B, C); and 3) multiciliated ependymal cells that were nestin-, caveolin 1–, and βIV-tubulin positive (Fig. 1B, C, I, J). At E20 and PN1, the VZ was formed by NSCs (~70%), nonciliated cells (~23%), and multiciliated cells (~7%). From PN1 onward, there were increasing numbers

FIGURE 1. In the hyHTx rat, disruption of the ventricular zone (VZ) starts during fetal life and continues during early postnatal life, resulting in the loss of neural stem cells (NSCs) and ependymal cells. The VZ is formed by 3 cell types: nonciliated cells, NSCs, and multiciliated ependymal cells. (**A**) Quantification of the 3 cell types at E20, PN1, and PN5. Data are shown as mean ± SE. * $p < 0.005$. (**B, C**) The 3 cell types are revealed by en bloc double immunolabeling for N-cadherin (green) and βIV-tubulin (red) (**B**) and scanning electron microscopy (SEM) (**C**). (**D**) Drawing depicting the 3 cell types of the VZ. (**E**) Section of the brain of a hydrocephalic E20 fetus. The disrupted VZ of the pallium (encircled) is shown in the following figures. The arrow points to the surface views using SEM and en bloc immunofluorescence (i.b.IF). (**F**) PN7 hydrocephalic HTx. Scanning electron micrograph of the roof of lateral ventricles. Most of the VZ of the pallium is disrupted (arrows in the left ventricle; asterisk in the right ventricle). (**G**) Immunostaining for nestin reveals NSCs (arrow); NSCs are missing at zones of disruption, and the subventricular zone (SVZ) is disorganized (broken line). (**H, J**) Disruption starts at different foci and progresses radially (green arrows). (**I**) Pallium of a hyHTx rat stained en bloc for βIV-tubulin displaying a focus of disruption where ependymal cells are missing. (**K**) Quantification of the area of VZ disruption in hyHTx rats. Data are shown as mean ± SE. * $p < 0.05$. Scale bars = (**B**) 3 μm; (**C**) 1.7 μm; (**E**) 1,000 μm; (**F**) 800 μm; (**G**) 65 μm; (**H**) 30 μm; (**I**) 25 μm; (**J**) 18 μm.

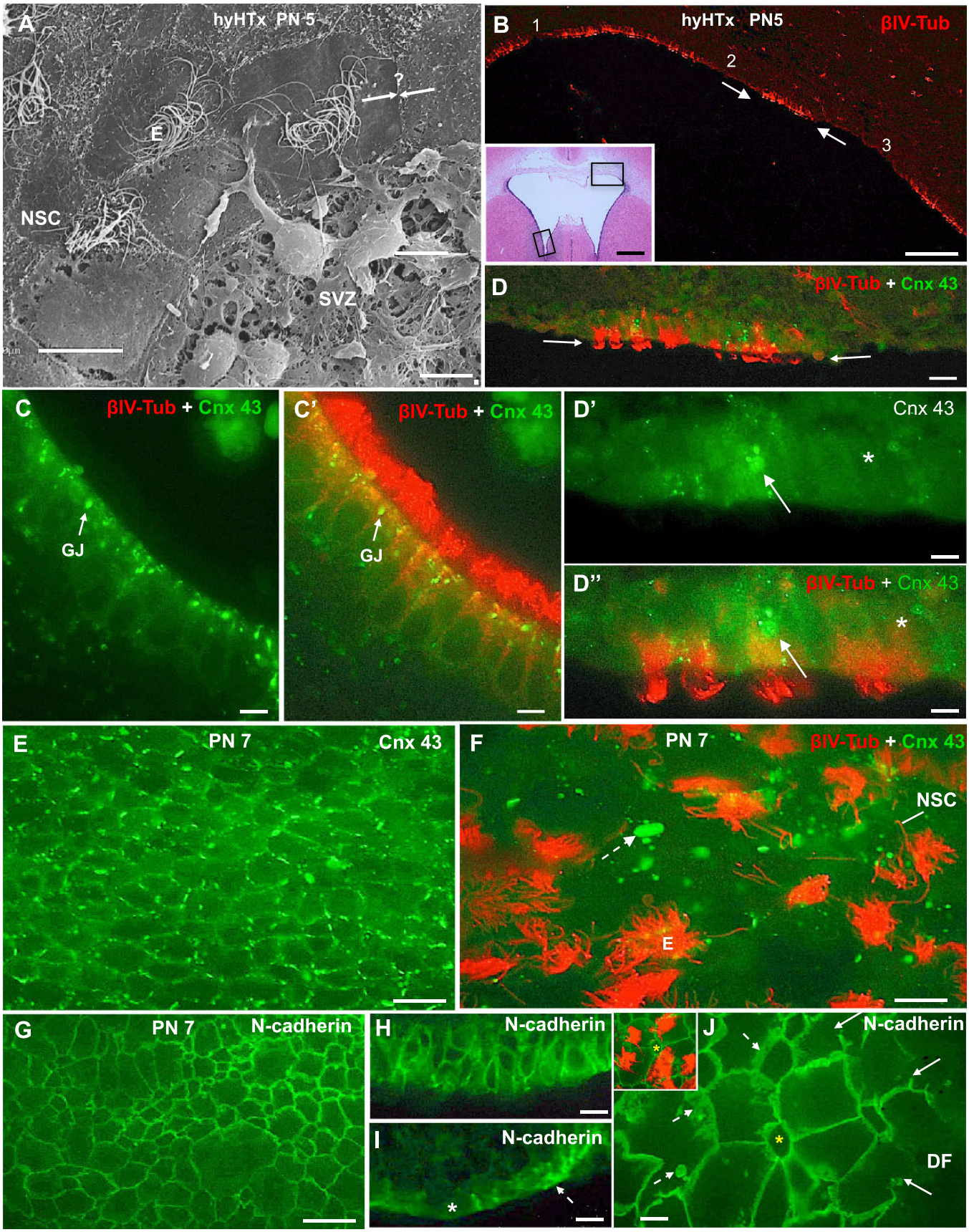

of multiciliated ependymal cells and a decreasing number of NSCs (Fig. 1A). Interestingly, the relative number of nonciliated cells remained approximately 20% during the periods studied. The possibility that they correspond to newborn NSCs not yet producing a cilium awaits investigation.

The VZ of the hyHTx Rat Telencephalon Undergoes Patterned Disruption

From E18 to PN7 hyHTx, disruption of the VZ consistently occurred in the dorsal wall of the lateral ventricles (pallium), rarely in the lateral wall, and never in the medial wall lined by multiciliated ependymal cells (Fig. 1E, F). Quantification of the denuded VZ area shows the progression of disruption from E19 to the end of the first postnatal weeks (Fig. 1K). Between PN7 and PN10, most of the VZ of the pallium had disrupted (Fig. 1F). During the first half of this 10-day period of disruption, most disrupted cells corresponded to NSC (Fig. 1A, G, H) whereas, during the second half, most disrupted cells were ependymal cells (Fig. 1A, I, J). The collective methodology, including CSF cell sampling, suggested the following sequence of events in disruption: phase 1, disruption starts as small foci where the VZ cells are missing and the NPCs of the SVZ protrude into the ventricle (Figs. 1J; 2A); phase 2, the disruption foci expand radially as the cells at the border (NSC or ependyma, depending on developmental stage) become denuded (Figs. 1H, J; 2A); and phase 3, expanding foci of disruption fuse and form large denuded areas (Fig. 1H, I).

The radial pattern of disruption makes HTx rats ideal to investigate the pathology of the VZ cells nearing disruption. The NSCs and ependyma have distinct phenotypes and certainly play different roles (6, 22). What do they have in common so that the disruption process will strike both cell types? We focused our attention on the expression of junction proteins in the VZ cells to understand this devastation.

Disrupted NSCs/Ependyma in hyHTx Rats Display Abnormal Expression of Junction Proteins

The VZ cells located at the disruption front of each denudation focus were the targets for analyzing the pathology leading to their injury (Fig. 2A, B). The cells bordering the disruption foci, soon to be detached, either accumulated connexin-43 and N-cadherin as large masses in the cytoplasm (arrow in Fig. 2D′, D″, F; broken arrow in Fig. 2I, J) or were devoid of these proteins (asterisks in the same figures). By contrast, the VZ of the lateral walls of the lateral ventricles did not disrupt, even under extreme ventricular expansion (Fig. 2B inset). In these latter cells, used as an internal control, similar to those of the VZ of nHTx, connexin-43 and N-cadherin localized at the apical region of the lateral plasma membrane (honeycomb appearance), most likely corresponding to gap and adherens junctions, respectively (Fig. 2C, C′, E, G, H).

VZ Disruption Leads to PH

From PN7 on, when rat corticogenesis has been completed and the VZ is mainly formed by multiciliated ependyma, PHs were consistently found in hyHTx rats (Fig. 3A–G). They were located at the roof of both lateral ventricles, at the sites where VZ disruption had taken place during the perinatal period (Figs. 1 F, G, E; 3A).

The cells forming PHs were either exposed to the ventricular cavity (Fig. 3D–F) or were partially or completely lined by a cell layer formed by GFAP-positive cells, ependymal cells, and a few cells with a long basal process (Fig. 3B). These processes arranged into bundles that divided PHs into compartments (Fig. 3B). This arrangement became more evident by tomato lectin binding that selectively labels the plasma membrane of NSCs (Fig. 3C). Periventricular heterotopias were formed by densely packed spherical cells, approximately 7 μm in diameter, displaying a large and strongly basophilic nucleus and a ring of cytoplasm (Fig. 3B).

At PN21, PHs became readily distinguishable (Fig. 3D–G). Virtually all cells forming PHs were βIII-tubulin positive and GFAP negative (Fig. 3F, G). Beta-III-tubulin–positive cells ranged in shape from spherical to small multipolar cells (Fig. 3E, F). After a cumulative dose of BrdU administered for 3 days, only 30% of the βIII-tubulin–positive cells of PHs displayed a labeled nucleus (Fig. 3E). By contrast, 80% to 90% of βIII-tubulin–positive cells of the postnatal neurogenesis SVZ were labeled with BrdU.

FIGURE 2. In hyHTx rats, the cells of the ventricular zone (VZ) close to become disrupted have abnormal connexin-43 and N-cadherin expression. (**A**) Scanning electron microscopy. Ependymal cells [E] and neural stem cells (NSCs) at the disruption borders were targeted for study of abnormalities of junction complexes (mirror arrows). (**B**) Disruption foci [1–3] are shown. Arrows point to disruption fronts approaching each other. For orientation, see the top rectangle of the insert. (**C, C′**) One- and 2-channel views to show connexin-43 (Cnx 43, green) and βIV-tubulin (βIV-tub, red) in an area not affected by disruption (for orientation, see bottom rectangle in inset of **B**); connexin-43 was confined to the plasma membrane forming gap junctions (GJ). (**D**) Two disruption fronts approaching each other (arrows). (**D, D′**) Detailed magnification of previous figure visualized with 1 and 2 channels for connexin-43 (green) and βIV-tubulin (red). Cells close to the disruption have cytoplasmic masses of connexin-43 (arrow) or lack this protein (asterisk). (**E**) En bloc immunostaining for connexin-43 of an unaffected area (for orientation, see bottom rectangle in inset of **B**). Connexin-43 is confined to the plasma membrane forming gap junctions. (**F**) Double en bloc immunostaining for connexin-43 (green) and βIV-tubulin (red) of an area undergoing disruption. Connexin-43 appears as cytoplasmic masses (broken arrow) located either in NSCs or multiciliated ependyma [E]. (**G**) En bloc immunostaining for N-cadherin of an unaffected area. A complete belt of N-cadherin surrounds each cell. (**H**) In tissue sections of unaffected areas, N-cadherin localizes at the lateral domain of the plasma membrane. (**I**) Cells close to disruption have cytoplasmic masses of N-cadherin (broken arrow) or lack this protein (asterisk). (**J**) En bloc immunostaining for N-cadherin in cells located at a disruption front (DF). The protein accumulates in the cytoplasm (broken arrow). The full arrows point to discontinuities of the N-cadherin belt. The VZ cells show some degree of spatial organization, with multiciliated cells surrounding a nonciliated cell (asterisk). The same group of cells visualized with 2 channels for N-cadherin (green) and βIV-tubulin (red) is shown in the inset. Scale bars = (**A**) 8 μm; (**B**) 70 μm, inset, 150 μm; (**C, C′**) 7 μm; (**D**) 15 μm; (**D′, D″**) 5 μm; (**E**) 10 μm; (**F**) 10 μm; (**G**) 10 μm; (**H**) 10 μm; (**I**) 15 μm; (**J**) 4 μm.

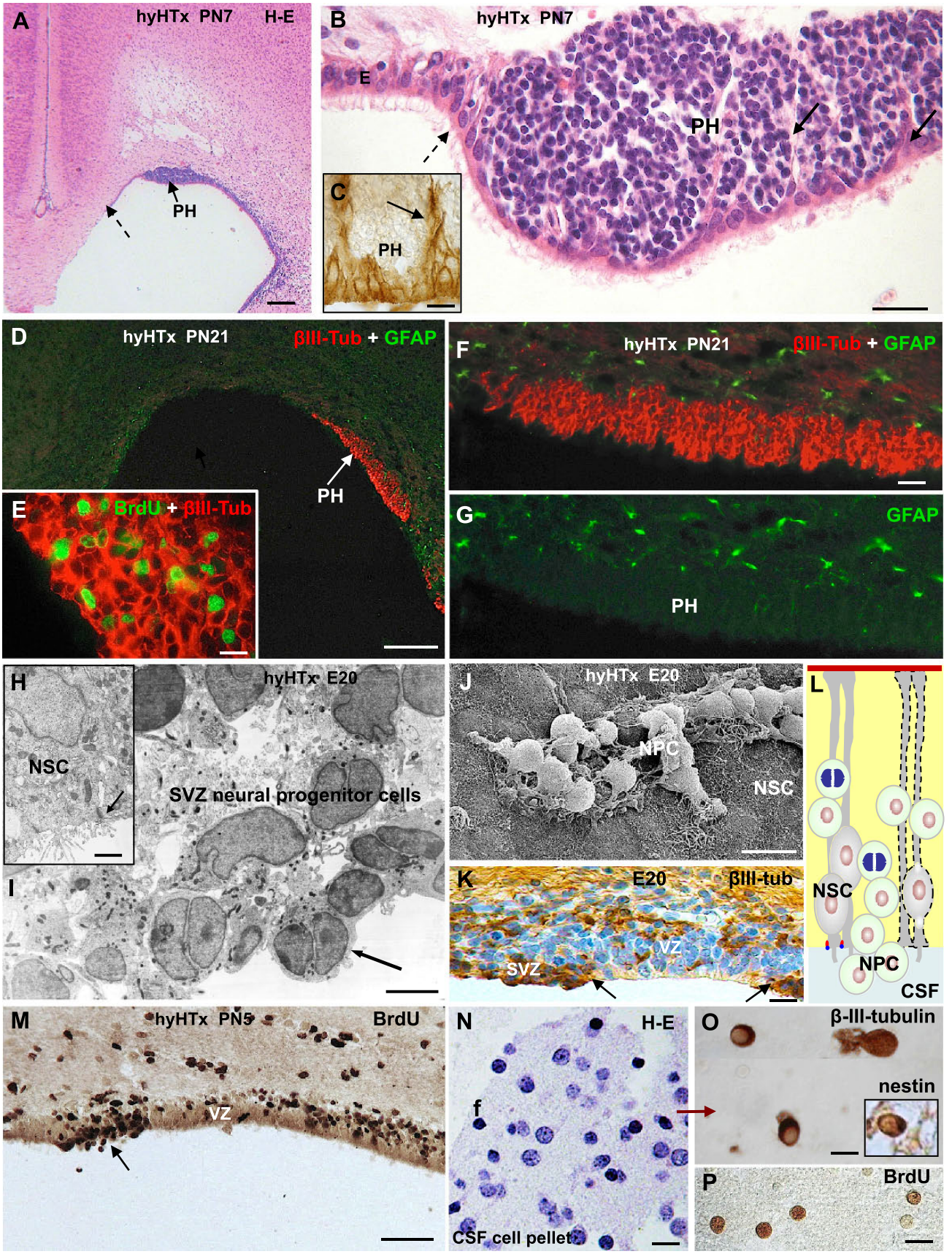

VZ Disruption Results in Abnormal Translocation of NSCs/NPCs Into Ventricular CSF

Immunocytochemical as well as transmission electron microscopy and SEM studies of hyHTx fetuses and newborns showed that NPCs reach the ventricles through the disrupted VZ (Fig. 3H–L). Bromodeoxyuridine administration during the first postnatal week in hyHTx rats showed labeled cells, most likely corresponding to NPCs, protruding through the disrupted VZ (Fig. 3M). Pellets of CSF collected from PN1 and PN5 hyHTx rats injected with BrdU revealed the presence of cells immunoreactive with antibodies against BrdU, βIII-tubulin, and nestin (Fig. 3N–P). These results indicate that proliferative NPCs, and probably NSCs, access the CSF. To test this hypothesis, we cultured these hyHTx cells to obtain neurospheres for comparison with those grown from the VZ/SVZ of nHTx and hyHTx.

NSCs/NPCs From CSF of hyHTx Rats Develop Into Neurospheres

Cerebrospinal fluid samples from hydrocephalic rats were processed for the neurosphere assay. Ten of 14 samples produced neurospheres ranging in size between 50 and 160 μm in diameter, with the largest population being approximately 100 μm diameter (Fig. 4A–G). Small and large neurospheres displayed distinct immunocytochemical characteristics (Fig. 4C–G). After 24-hour BrdU labeling, most labeled nuclei were located at the neurosphere surfaces (Fig. 4B). Nestin was also detected by immunoblotting in neurospheres grown for 4 and 6 DIV (Fig. 4D). Neurospheres grown from cells of hyCSF indicate that the NSCs/NPCs abnormally translocated to the CSF retained their capacity to proliferate and assemble. No neurospheres were obtained from the CSF of nHTx rats.

Neurospheres Formed by NSCs/NPCs From hyHTx Rat CSF Express Similar Cell Junction Abnormalities as VZ Cells Undergoing Disruption

Neurospheres obtained from the VZ/SVZ of nHTx rats (Fig. 4I–M) and from the CSF of hyHTx rats (Fig. 4N–R) were cultured in parallel and photographed under phase contrast microscopy twice daily for 7 consecutive days. After 2 DIV, hyCSF-derived neurospheres started to disassemble, resulting in numerous cells becoming free in the culture medium (Fig. 4N–Q). After 6 and 7 DIV, most neurospheres had disassembled into numerous free isolated cells, some of which proliferated to form new neurospheres (Fig. 4P, Q, insets). When processed for light microscopy, these neurospheres displayed cells ''disrupting'' from the cortex (Fig. 4R).

The cells of neurospheres obtained from hyCSF did not display N-cadherin at the plasma membrane domain but accumulated this protein in the cytoplasm (Fig. 4T, W). This clearly contrasted with the honeycomb appearance of N-cadherin in neurospheres obtained from the VZ/SVZ of nHTx rats (Fig. 4S, S′, U). This phenomenon became more evident after microdensitometric recordings (Fig. 4V). These findings indicate that 1) the NSCs/NPCs reaching the CSF (although they did disrupt because of a junction pathology) can proliferate and become assembled again through adherens junctions when put into culture, and 2) a few days are necessary for the neurospheres to express the abnormalities and become disrupted.

Neurospheres From the VZ/SVZ of hyHTx Rats Have Abnormalities Resembling Those of Neurospheres Obtained From hyCSF

After 6 DIV, neurospheres developed from the VZ/SVZ of nHTx were formed by densely packed proliferative cells (Fig. 5A, C). Although nestin-positive cells distributed throughout the neurosphere, they were preferentially located at the periphery of the neurospheres (Fig. 5E, F), with their processes projecting to the central zone (or core) (Fig. 5B). A few βIII-tubulin–positive cells displaying processes of different thicknesses and lengths and numerous spherical and multipolar GFAP-positive cells (i.e. differentiating astroblasts) populated the cores of the neurospheres (Fig. 5C, F). The neurosphere cells, particularly those at the periphery, were joined together by N-cadherin–based adherent junctions (Figs. 4S; 5D). Six DIV neurospheres from the VZ/SVZ of nHTx, processed for the differentiation assay, differentiated into multipolar βIII-tubulin–positive neurons and multipolar GFAP-positive astrocytes (Fig. 5G).

The NSCs/NPCs from the VZ/SVZ of hyHTx rats produced neurospheres of different sizes and characteristics. Large neurospheres were approximately 200 to 300 μm in diameter, with a core of loosely packed cells and a cortex with densely packed cells (Fig. 5H). The cortex was formed by proliferative (Fig. 5I) nestin-positive (Fig. 5L) cells. The cores

FIGURE 3. In the HTx rat, disruption of the ventricular zone (VZ) results in periventricular heterotopias (PHs) (**A**–**G**) and shedding of neural progenitor cells into the CSF (**H**–**P**). (**A**) PHs located close to a disruption front (arrow). (**B**) PH located under a cell layer formed by multiciliated cells and cells with a basal process (broken arrow); these processes divide the PH into compartments (full arrows). (**C**) Adjacent section processed for tomato lectin binding. Arrow points to bundles of basal processes of the cells in the VZ. (**D, E**) PHs are formed by βIII-tubulin (βIII-tub)–positive cells, some of which are proliferative and stain for bromodeoxyuridine (BrdU). GFAP, glial fibrillary acidic protein. (**F, G**) PHs visualized with 2 channels for GFAP (green) and βIII-tubulin (red) (**F**) and with only the channel for GFAP (green). (**H**–**K**) Transmission electron microscopy of unaffected neural stem cells (NSCs) (**H, I**); arrow points to an adherens junction. Cells displaced to the ventricle through a disruption point were identified as NPCs (arrows) by transmission electron microscopy (**I**), scanning electron microscopy (**J**), and immunocytochemistry for βIII-tubulin (**K**). (**L**) Line drawing depicting the pathology of hyHTx: loss of NSCs (outlined by broken line) and translocation of NPCs to the CSF. (**M**–**P**) Cells displaced to the ventricle and reaching the CSF retain the proliferative capacity, as shown by injection of BrdU in living animals and tracking the BrdU-positive cells in tissue sections (**M**, arrow) and CSF cell pellets (**N, P**). Cell pellet of CSF collected from a PN1 hyHTx rat is shown in **N**. Beta-III-tubulin–positive or nestin-positive cells were present in the cell pellet (**O**). Scale bars = (**A**) 125 μm; (**B**) 35 μm; (**C**) 10 μm; (**D**) 125 μm; (**E**) 10 μm; (**F, G**) 20 μm; (**H**) 3 μm; (**I**) 5 μm; (**J**) 12 μm; (**K**) 14 μm; (**M**) 50 μm; (**N**) 10 μm; (**O**) 8 μm; (**P**) 10 μm.

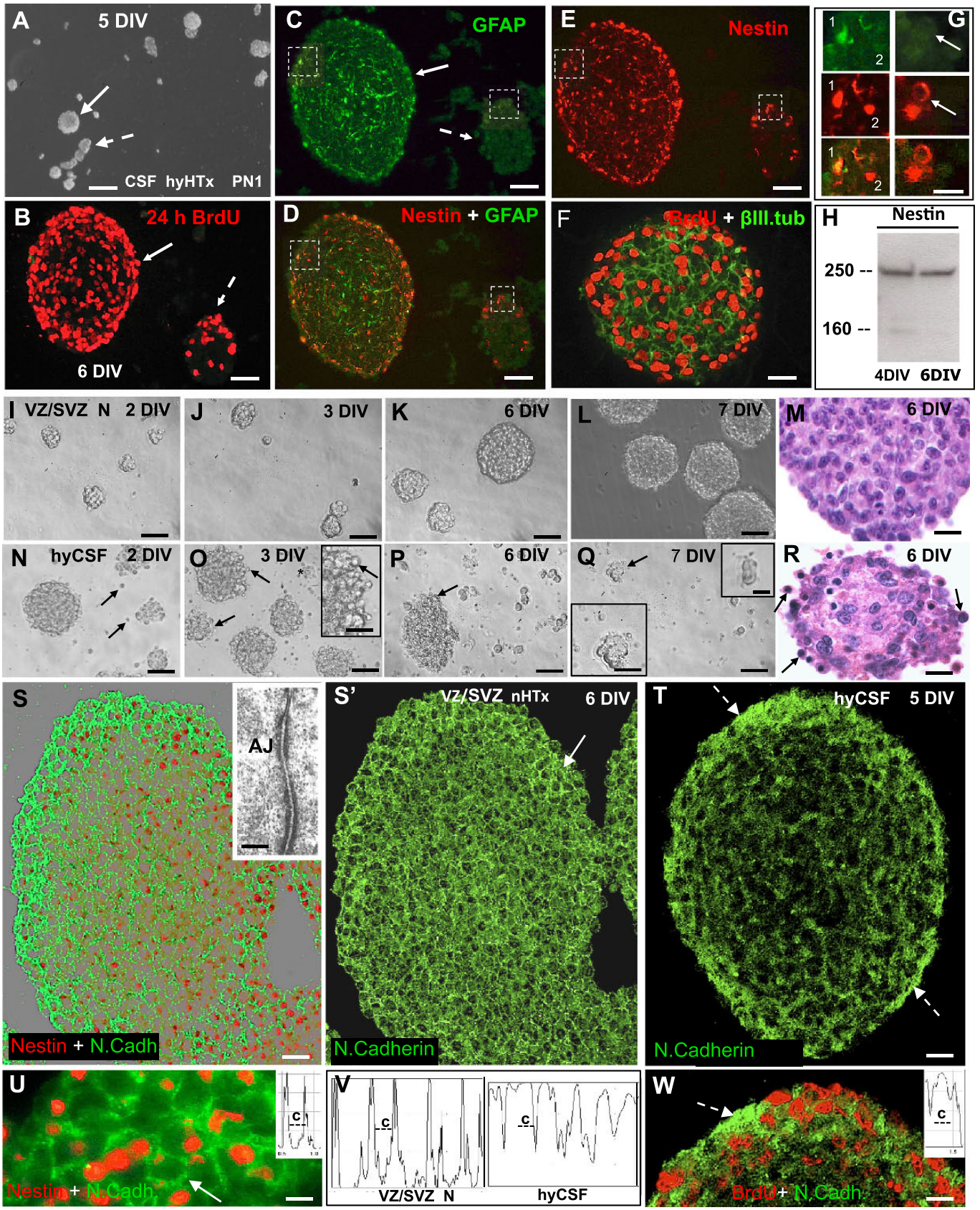

were devoid of proliferative cells and were populated by numerous multipolar βIII-tubulin–positive cells (Fig. 5M), with only a few GFAP-positive cells. Smaller neurospheres, approximately 40 to 100 μm in diameter, were formed by densely packed cells with strongly labeled BrdU-positive nuclei distributed throughout (Fig. 5I). Nestin-positive cells and spherical βIII-tubulin–positive cells were evenly distributed (Fig. 5L, M). These characteristics suggest that small neurospheres are younger than large neurospheres, and they are born from cells disrupting from large neurospheres. This possibility is supported by findings under phase contrast microscopy (inset, Fig. 5H) and by the abnormal subcellular location of N-cadherin (Fig. 5J, K). After 6 DIV, neurospheres from the VZ/SVZ of hyHTx rats processed for the differentiation assay differentiated into multipolar βIII-tubulin–positive neurons and multipolar GFAP-positive astrocytes (Fig. 5N), indicating that, despite their junction pathology, hydrocephalic NSCs retained the potential for differentiation into neuron and glia.

Human Hydrocephalic Fetuses Also Display Disruption of the Telencephalic VZ and Abnormal Junction Protein Expression

In the telencephalon of control human fetuses, a temporospatial pattern of VZ differentiation resembling that of the rat was observed. In 16, 21, and 22 GW fetuses, the VZ of the telencephalon was formed by NSCs and few multiciliated ependymal cells (Fig. 6A, A′, B, B′). In 25 and 30 GW fetuses, one wall of the lateral ventricle was lined by ependyma and the other by NSCs; both cell types had N-cadherin at the plasma membrane (Fig. 6C, C′, D). In the 33 to 40 GW fetuses, the wall of the lateral ventricle was mostly formed by multiciliated mature ependyma.

In hydrocephalic fetuses, the VZ cells, either NSCs or ependyma, underwent disruption. In young hydrocephalic fetuses (21, 22 GW), disruption occurred in the pallium whereas, in 40-week fetuses, the disruption extended to other regions of the lateral ventricles (Figs. 6E; 7A, B, D). Ependymal cells close to a disrupted area (probably corresponding to candidate cells for disruption) accumulated N-cadherin and caveolin 1 as large masses in the cytoplasm (Fig. 6G, I, I′). By contrast, the ependymal cells of control fetuses (Fig. 6C, D, H) and those of the nondisrupted regions of the hydrocephalic fetuses (Fig. 6F) localized N-cadherin at the lateral domain of the plasma membrane and caveolin 1 close to the apical and basal domains of the plasma membrane.

Disruption of the VZ in Human Hydrocephalic Fetuses Leads to Abnormal Migration of NPCs and Neuroblasts

In human hydrocephalic fetuses, VZ disruption was associated with several abnormalities, as follows: 1) βIII-tubulin–positive cells in the SVZ (Fig. 7F) were translocated into the ventricle at the sites of VZ disruption (Fig. 7A′, A″, B, D, G). 2) Subependymal rosettes formed close to the site of VZ disruption were composed of GFAP-positive cells with long basal processes and displayed little or no N-cadherin (Fig. 7B, D, H, I). 3) Periventricular heterotopias formed close to the site of VZ disruption consisted of βIII-tubulin–positive neuroblasts arrested near the SVZ (Fig. 7A–C). The neighboring disrupted VZ was covered with a layer of astrocytes, indicating that the disruption and PH formation had occurred earlier in development (Fig. 7C). Periventricular heterotopias were already found in the 21 GW embryo (Fig. 7A, A′), as well as in full-term fetuses (40 GW) (Fig. 7C). 4) In 3 hydrocephalic fetuses, large clusters of βIII-tubulin–positive cells were seen within the perivascular space, far from the ventricle, suggesting that in the absence of radial glia, a bulk of neuroblasts used blood vessels as scaffold for migration (Fig. 7B, B″).

DISCUSSION

Fetal-onset hydrocephalus is heterogeneous, and genetic and environmental factors, such as vitamin B or folic acid deficiency (3), viral infection of ependyma (4), and prematurity-related germinal matrix and intraventricular hemorrhage (5), contribute to its occurrence. The association between onset and evolution of congenital hydrocephalus and stenosis/obliteration of the aqueduct of Sylvius is somewhat controversial. There are reports indicating that morphologic abnormalities of the aqueduct account for a low percentage (10%–25%) of fetal hydrocephalus (27, 28). However, there are several types of neural tube

FIGURE 4. (**A**) Neural stem cells/neural precursor cells (NSCs/NPCs) collected from the CSF of a PN1 hyHTx rat form small (broken arrows) and large (full arrows) neurospheres. DIV, days in vitro. (**B**) The neurospheres contain bromodeoxyuridine (BrdU)-positive proliferative cells. (**C**–**F**) Large neurospheres contain nestin-positive cells located at the periphery (**D, E**) and a few glial fibrillary acidic protein (GFAP)–positive (**C, D**) and numerous βIII-tubulin (βIII.tub)–positive cells at the core (**F**). Small neurospheres contained βIII-tubulin–positive cells and lacked GFAP-positive cells (**C**, broken lines). (**G**) Detailed magnification of areas framed by squares in **C**, **D**, and **E**. (**H**) Immunoblot for nestin of neurospheres collected after 4 and 6 DIV. (**I**–**Q**) Phase contrast microscopy of living neurospheres from the ventricular zone/subventricular zone (VZ/SVZ) of a nonhydrocephalic (nHTx) rat after 2, 3, 6, and 7 DIV (**I**–**L**) and from the CSF of PN1 hyHTx rats after 2, 3, 6, and 7 DIV (**N**–**Q**). From 2 DIV on, neurospheres from the CSF started to disassemble (arrows). At 7 DIV (**Q**), isolated cells and small growing neurospheres, most likely formed by disrupted cells, started to appear (arrow). Top inset, dividing cell; bottom inset, small growing neurosphere. Paraffin section of a neurosphere from VZ/SVZ of an nHTx rat (**M**). (**R**) Paraffin section of a neurosphere from hydrocephalic rat CSF (hyCSF), similar to that shown in (**D**); it had an irregular outline, with cells ''disrupting'' from its periphery (arrows). (**S, S′, U**) In neurospheres from the VZ/SVZ of an nHTx rat, N-cadherin was located at the plasma membrane domain, forming a continuous belt. This is also shown in the microdensitometric recording (**V**, left panel) (c, cytoplasm). Inset in (**S**), transmission electron microscopy showing neurosphere cells joined by adherens junctions (AJ). (**T, W**) Neurospheres from hyCSF expressed abnormalities of N-cadherin similar to those expressed by NSCs of mutant animals. N-cadherin accumulated in the cytoplasm of neurosphere cells (broken arrows). This is also shown in the microdensitometric recording (**V**, right panel). Scale bars = (**A**) 125 μm; (**B**–**E**) 25 μm; (**F**) 15 μm; (**G, M, R**) 10 μm; (**I**–**L**, **N**–**Q**) 50 μm; (**S**, **S′**,**T**) 20 μm; (**U**, **W**) 8 μm.

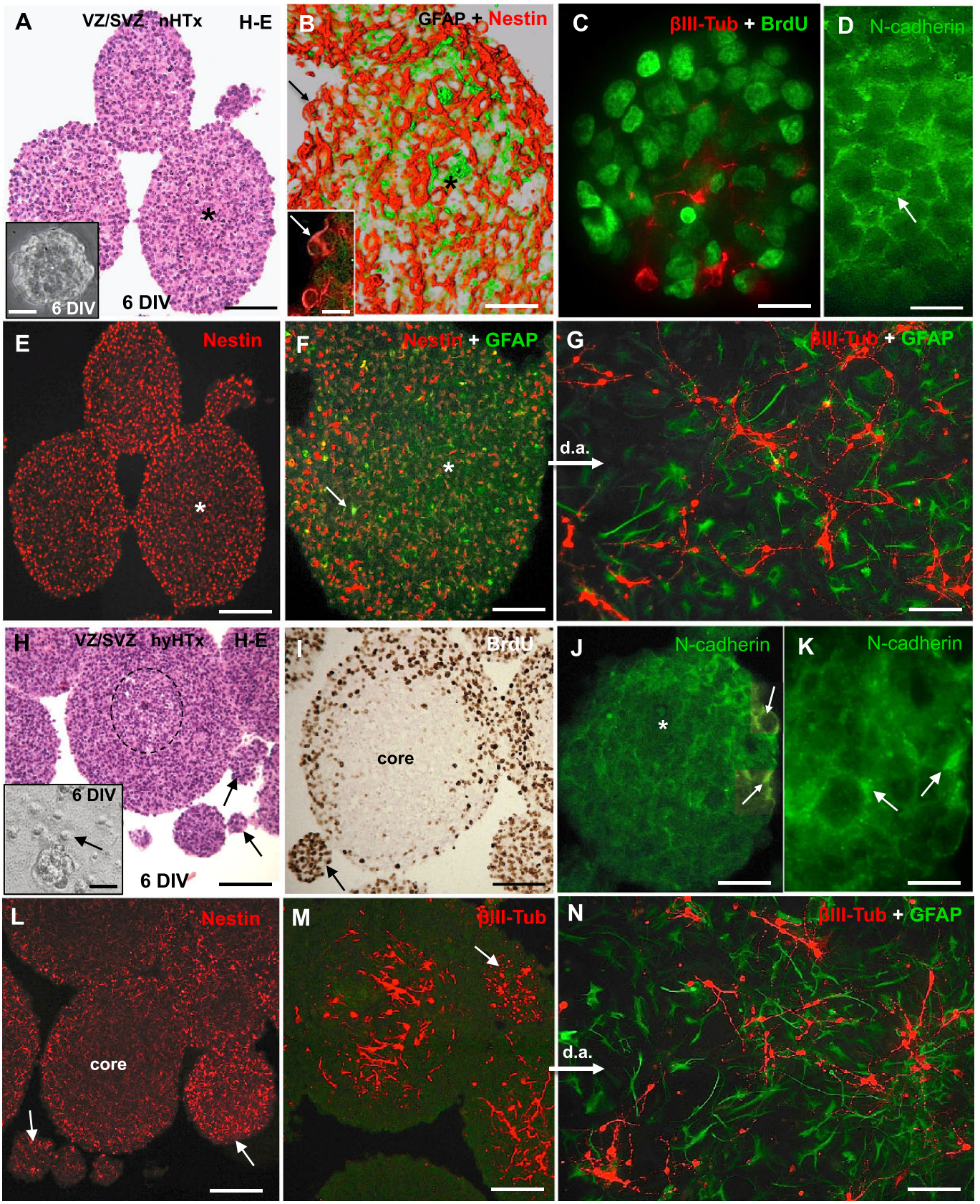

defects that are associated with both congenital hydrocephalus and aqueductal stenosis, indicating that both phenomena are more intimately associated than formerly thought. There is an X-linked syndrome, occurring in approximately 1:30,000 births, characterized by congenital hydrocephalus and stenosis of the aqueduct, and 25% of males with aqueductal stenosis have X-linked hydrocephalus (1). Although no other gene mutations associated with aqueduct stenosis and hydrocephalus have been identified in humans, a long series of gene mutations in mice that trigger aqueduct stenosis and hydrocephalus has been reported in recent years (9).

Spina bifida, a distal neural tube defect, is associated with a wide range of CNS malformations, the most frequent being the obstruction of CSF flow within the ventricular system (92%) and a disorder of migration of cortical neurons (92%) (2). Gilbert et al (2) postulated that spina bifida and brain malformations must be considered part of a spectrum of malformations caused by an unidentified primary CNS insult. However, there is no agreement with respect to the degree of association between spina bifida and aqueductal stenosis (3, 27–31). In this respect, it is worth considering that, in animal models of congenital hydrocephalus, aqueduct stenosis is a process starting in fetal life and finishing early after birth (17–19). There is evidence that this process may also occur in human congenital hydrocephalus (15, 16). Therefore, the presence or absence of aqueduct stenosis depends on the developmental stage under investigation. Furthermore, a patent aqueduct may display a functional stenosis derived from disruption of the multiciliated ependyma (16).

Recent investigations focused on the cellular and molecular phenomena underlying fetal-onset hydrocephalus have brought new insights to this pathologic spectrum. Studies on numerous mutant animal models indicate that a disruption of the VZ of the aqueduct, starting early in development, triggers aqueduct stenosis and hydrocephalus (17–19). A similar phenomenon seems to take place in cases of human congenital hydrocephalus (15, 16).

The evidence strongly indicates that fetal-onset hydrocephalus is not only an alteration of CSF dynamics but also a brain disorder that is triggered by multiple factors. How can we explain why surgery does not reverse the neurologic impairment suffered by neonates with fetal-onset hydrocephalus? The present findings indicate that fetal-onset hydrocephalus and abnormal neurogenesis should be regarded as 2 inseparable phenomena because they share a common origin: a primary pathology of the VZ (Fig. 8). It is tempting to suggest that VZ disruption would be the ''unidentified primary insult to the CNS'' leading to distal neural tube defects and brain malformations, as suggested by Gilbert et al (2).

The process of VZ disruption, first affecting the cerebral aqueduct, also reaches the telencephalon (15, 17–19, present report). We investigated VZ disruption in the telencephalon of both mutant HTx rats and human hydrocephalic fetuses. Our data support the notion that cell junction abnormalities of VZ cells of the telencephalon lead to both VZ disruption and neurogenesis abnormalities.

The VZ and SVZ are the source of most cells of the brain. With the exception of microglia, all other cells of the developing brain originate in the VZ and SVZ (Fig. 9A) (12–14, 32, 33). The VZ contains multipotent NSCs that are bathed in the fetal CSF and project long basal processes that reach the pial surface (Fig. 9A). A hallmark of NSCs is their primary cilia, which project to the ventricle (34, 35). Neural stem cells progressively differentiate into multiciliated ependyma (1). In rodents, differentiation of ependyma starts late in development and is completed by the first postnatal week (16, 36, present report). In humans, ependymal cell differentiation starts at about the fourth week of gestation and is completed around the 22nd gestational week (37, 38). The SVZ contains the neural precursors, which lose contact with the ventricular

FIGURE 5. Neurospheres from the ventricular zone/subventricular zone (VZ/SVZ) of hyHTx rats have abnormalities resembling those of neurospheres from the CSF of hyHTx rats. Paraffin sections of neurospheres from the VZ/SVZ of PN1 nonhydrocephalic (nHTx) rats after 6 days in vitro (DIV) (**A**–**F**) and from the VZ/SVZ of PN1 hyHTx rats after 6 DIV (**H**–**M**). (**A**) Neurospheres from an nHTx rats stained with hematoxylin and eosin. The asterisk indicates the same neurosphere shown in **B**, **E**, and **F**. Inset: Phase contrast microscopy of a living neurosphere from an nHTx rat displaying a compact appearance. (**B**) Reconstruction of confocal z-axis images of a neurosphere double immunolabeled for nestin (red) and glial fibrillary acidic protein (GFAP, green). The network of neural stem cells and their processes is evident. The arrows point to the same cell shown in the inset in a z-axis through the cell body and its process (inset). (**C**) Neurosphere immunolabeled for bromodeoxyuridine (BrdU, green) and βIII-tubulin (red). Most nuclei are BrdU positive. The few βIII-tubulin–positive cells project processes of different thicknesses and lengths. (**D**) Neurosphere immunolabeled for N-cadherin. The protein is confined to the plasma membrane domain, forming a continuous belt (arrow). (**E**) Section adjacent to that of (**A**). Nestin-positive cells are preferentially located at the periphery of neurospheres. (**F**) Section adjacent to that of (**E**). Nestin-positive cells (red) concentrate at the periphery, whereas spherical and multipolar GFAP-positive cells (green, differentiating astroblasts) start to populate the core of neurospheres (arrow). (**G**) Six DIV neurospheres processed for the differentiation assay (d.a.) differentiate into multipolar βIII-tubulin–positive neurons (red) and multipolar GFAP-positive astrocytes (green). (**H**) Neurospheres from hyHTx rats, showing small (arrows) and large neurospheres; the latter have a core of loosely arranged cells (broken circle). Inset. Phase contrast microscopy of a small living neurosphere from an hyHTx rat with numerous isolated cells in the vicinity (arrow). (**I**) In large neurospheres, BrdU-positive nuclei are confined to the periphery, whereas the core is free of proliferating cells. All nuclei of small neurospheres are strongly BrdU positive (arrow). (**J, K**) Neurosphere from an hyHTx rat immunolabeled for N-cadherin. The protein appears as cytoplasmic masses in many cells (arrows) whereas, in others, N-cadherin is missing (asterisk). (**L**) In large neurospheres, nestin-positive cells are confined to the periphery whereas, in small neurospheres, they are distributed throughout (arrow). (**M**) In large neurospheres, numerous multipolar βIII-tubulin–positive cells populate the core (asterisk), whereas spherical βIII-tubulin–positive cells are distributed throughout in small neurospheres (arrow). (**N**) Six DIV neurospheres processed for the d.a. differentiate into multipolar βIII-tubulin–positive neurons (red) and multipolar GFAP-positive astrocytes (green). Scale bars = (**A**) 80 μm, inset, 15 μm; (**B**) 38 μm, inset, 15 μm; (**C**, **D**) 15 μm; (**E**) 80 μm; (**F**) 42 μm; (**G**) 60 μm; (**H**) 115 μm, inset, 24 μm; (**I**) 70 μm; (**J**) 40 μm; (**K**) 20 μm; (**L**) 115 μm; (**M**) 60 μm.

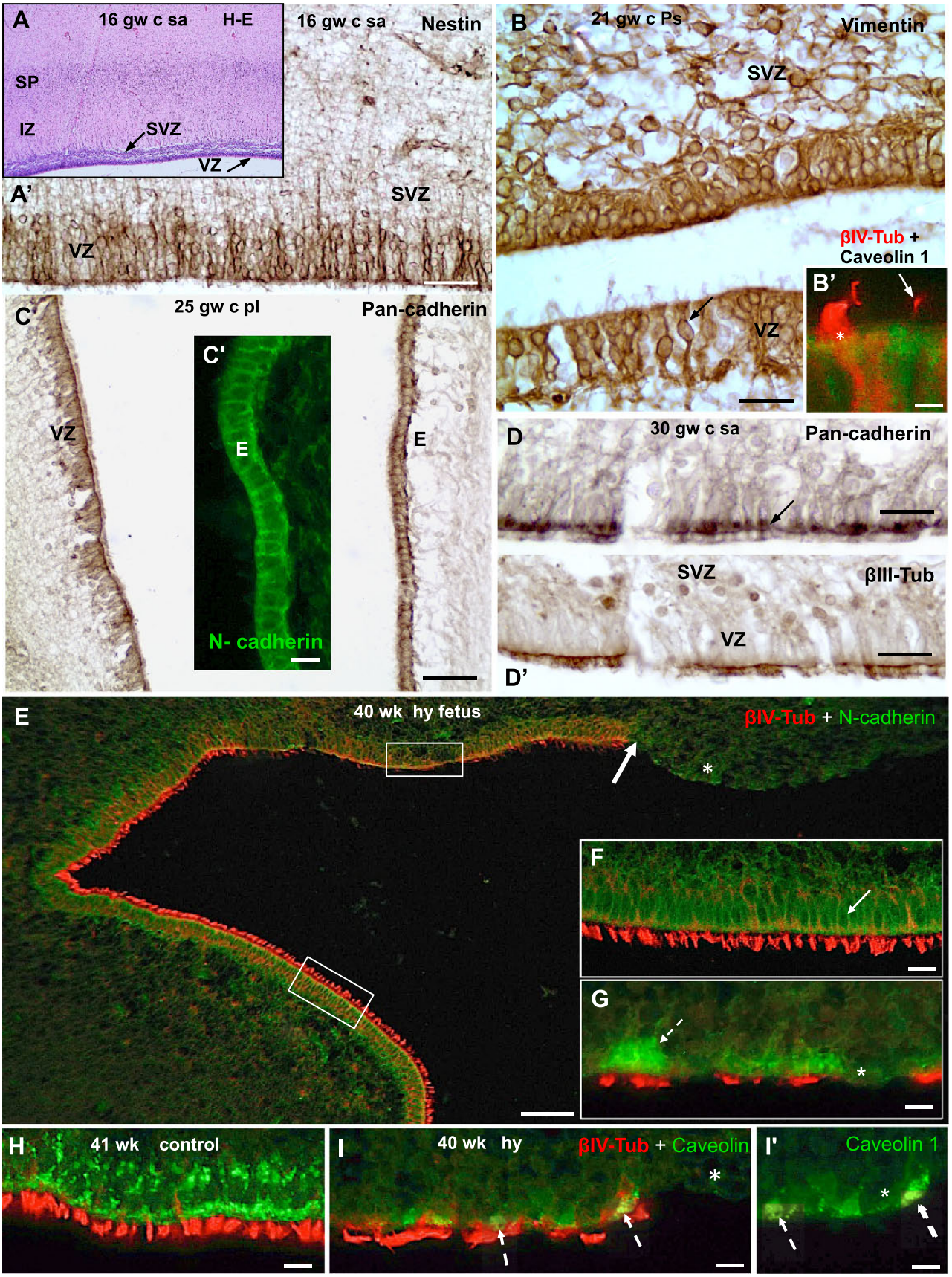

surface, proliferate extensively, and then differentiate into neuroblasts that migrate using the basal process of NSCs as scaffolding (Fig. 9A) (33, 39).

The Mutation of a Wide Spectrum of Genes May Lead to VZ Disruption

The disruption of the VZ follows a program that has temporal and spatial patterns, progressing as a ''tsunami'' wave, leaving behind severe damage (9, 17–19). Ventricular zone disruption starts at early embryological stages when this zone is formed by the NSCs (17–19) and continues during developmental stages when the VZ is formed by multiciliated ependyma (40, present findings). Although the disruption process affects both cell lineages equally, NSCs are affected during the key initial stages of the pathology. The loss of NSCs/ependyma occurs at specific regions of the Sylvian aqueduct and ventricular walls and at specific stages of brain development. This explains why only certain brain structures have abnormal development, which, in turn, results in specific neurologic impairments.

Disruption of the VZ occurs in human hydrocephalic fetuses (15, 16) and in a series of mutant mice, each one carrying a mutation for apparently nonrelated proteins, such as αSnap (17, 41, 42), Lgl1 (43), atypical protein kinase C-lambda (aPKCλ) (44), and nonmuscle myosin II-B (NMII-b) (45). What do such a variety of gene mutations have in common so that they all result in VZ disruption?

Intercellular Junction Abnormalities of NSCs/Ependymal Cells Are a Final Common Pathway of Gene Mutations That Lead to VZ Disruption

Several studies indicate that disruption of the VZ arises from a final common pathway involving alterations of vesicle trafficking, abnormal cell junctions, and loss of VZ integrity (20, 43–46, present report). Our findings of abnormal localization of N-cadherin and connexin-43 in NSCs/ependymal cells and the formation of subependymal rosettes suggest that VZ disruption results from a defect in cell polarity and in cell-to-cell adhesion of VZ cells. This view is in line with reports on the role of N-cadherin for maintaining the normal architecture of the neuroepithelium and NSCs (44–47). Up to E12, neuroepithelial cells are joined together by gap, adherens, and tight junctions (9, 34, 35). From E12 onward, when neuroepithelial cells differentiate into NSCs, tight junctions are missing and cell-to-cell adhesion of NSCs relies on gap and adherent junctions. It is exactly at this time when disruption of the VZ starts in mutant hyh mice (17). Interestingly, specific domains of the ventricular walls that are permanently endowed with tight junctions, such as the subcommissural organ, choroid plexus, and hypothalamic tanycytes, never disrupt (19).

The accumulation of N-cadherin and connexin-43 in the soon-to-detach VZ cells in HTx rats and their virtual absence from the plasma membrane (present report) suggest that these molecules are synthesized but are not properly transported to the plasma membranes of the cells. The mechanism involved in this abnormal expression and translocation of N-cadherin is unknown. Knockout of PTB, an RNA-binding protein expressed in NSCs, induces the gradual loss of adherens junctions in the VZ, then VZ disruption and hydrocephalus onset (11). The Numb and Numbl proteins are required for maintaining adherent junctions in NSCs; Numb and Numbl double-knockout animals develop hydrocephalus (46). The specific disruption of N-cadherin–based junctions is enough to induce ependymal disruption. Indeed, the use of N-cadherin antibodies or synthetic peptides harboring a cadherin-recognition sequence triggers the detachment of ependymal cells from explants of the dorsal wall of the Sylvian aqueduct (21). The abnormal localization of connexin-43 in NSCs/ependymal cells could be associated with the faulty localization of N-cadherin. Indeed, it has been reported that gap junction proteins are delivered to the plasma membrane at adherent junction sites (48).

The nature of the genetic defect expressed in the HTx rat and in hydrocephalic patients (15–19) is unknown. We postulate that they all carry a defect at one or another point of the pathways assembling adherens and gap junctions, but non-genetic mechanisms leading to VZ disruption also have to be considered (49, 50). Indeed, lysophosphatidic acid, a blood-borne factor found in intraventricular hemorrhages, binds to receptors expressed by the VZ cells and triggers VZ disruption and hydrocephalus (49). Vascular endothelial growth factor is elevated in the CSF of patients with hydrocephalus and, when it is administered into the CSF of normal rats, it causes alterations of adherens junctions, ependyma disruption, and hydrocephalus (50). Thus, the possibility that signals from the hydrocephalic CSF may contribute to, or even trigger VZ disruption, has to be kept in mind. Furthermore, fetal CSF is the internal milieu of NSCs playing a key role on brain development (51), and the CSF of hyHTx rats has an abnormal protein

FIGURE 6. (**A**–**D′**) Control (nonhydrocephalic) human fetuses at 16 (**A, A′**), 21 (**B, B′**), 25 (**C, C′**), and 30 (**D, D′**) gestational weeks (GW) of age showing normal ventricular zone (VZ) and subventricular zone (SVZ). sa, spontaneous abortion; Ps, Potter syndrome; pl, premature labor. (**A**) Pallium stained with hematoxylin and eosin [H-E]. The VZ, SVZ, intermediate (IZ) zone, the subplate (SP), and the cortical plate (CP) were readily distinguishable. The cells of the VZ were strongly reactive for nestin (**A′**), and cadherin was located at the lateral plasma membrane domain (**C′**). (**B**) In the 21 GW control fetus, the cells of the VZ were strongly reactive for vimentin. At this stage, multiciliated (asterisk) and monociliated (arrow) cells were readily distinguishable using antibodies against βIV-tubulin (βIV-tub) (**B′**). The integrity of the VZ and SVZ was also revealed in the 25 and 30 GW fetuses using antibodies for pan-cadherin (**D**) and βIII-tubulin (**D′**). Cells of the VZ displayed pan-cadherin and N-cadherin at the lateral plasma membrane domain, especially at the apical cell pole (arrow in **D**). Ependyma [E]. (**E**) Pallium of a human hydrocephalic fetus showing zones lined by normal (lower rectangle) or abnormal (upper rectangle) ependyma. Asterisk, denuded area; arrow, disruption front. The areas framed are shown in (**F**) and (**G**). Close to the disruption front, ependymal cells displayed abnormal expression of N-cadherin (**G**) and caveolin 1 (**I, I′**) (broken arrows, asterisks). In areas of intact ependyma, N-cadherin is localized at the plasma membrane (**F**, arrow); caveolin 1 is confined to both cell poles (**H**). Scale bars = (**A**) 160 μm; (**A′**, **F**) 20 μm; (**B**, **E**) 30 μm; (**B′**, **H**, **I**, **I′**) 7 μm; (**C**) 30 μm; (**C′**) 12 μm; (**D**, **D′**) 24 μm; (**G**) 10 μm.

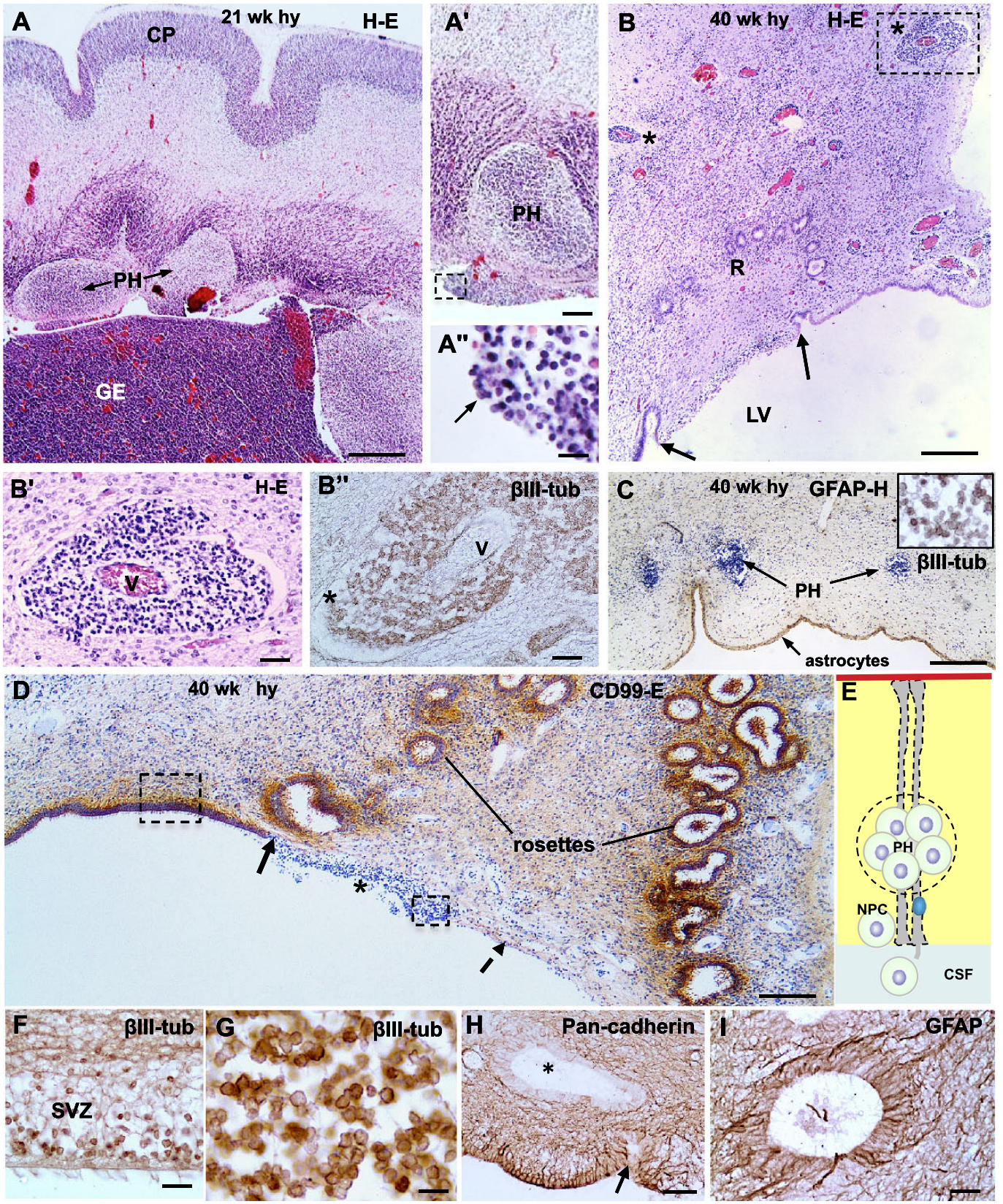

composition, which might contribute to the abnormal neurogenesis that occurs in this mutant (52–55).

Outcomes of the Disruption of NSCs/Ependymal Cells: Hydrocephalus and Abnormal Neurogenesis

In the hyh mouse, programmed disruption of the VZ of the ventral wall of the Sylvian aqueduct starts early in fetal life (E12.5) and precedes the onset of a communicating hydrocephalus. The loss of the ependyma of the dorsal wall of the aqueduct occurring shortly after birth leads to fusion of the denuded ventral and dorsal walls of the aqueduct, aqueduct obliteration, and severe hydrocephalus (17–19). Ventricular zone disruption associated with the onset of hydrocephalus has also been found in other mutant mice (43–46, 56) and in spontaneously aborted fetuses (16). Thus, disruption of the VZ in the aqueduct of Sylvius leads to hydrocephalus.

In human hydrocephalic fetuses and the HTx rat, the VZ disruption results in 2 neuropathologic events: formation of PH and translocation of NSCs/NPCs to the CSF (Fig. 9B). It seems likely that, at regions of disruption where NSCs have been lost, the neuroblasts generated in the SVZ no longer have the structural scaffolding to migrate and consequently accumulate in periventricular areas to form PH. The facts that PHs are present in adult HTx rats and that they are formed mostly by βIII-tubulin–positive cells with a low rate of proliferation indicate that these cells likely correspond to arrested neuroblasts. In the human hydrocephalic fetuses studied, PHs were found in young (21 GW) and full-term (40 GW) fetuses, indicating that they likely were formed early in development and had remained in situ until the end of fetal life and probably after birth. Indeed, a 2-month-old child with a disrupted VZ had PHs (20). Periventricular heterotopias behave as epileptogenic foci (57), and epilepsy affects 6% to 30% of congenital hydrocephalus patients (58, 59).

In 3 of the human hydrocephalic fetuses studied, large clusters of βIII-tubulin–positive cells were seen within the perivascular space, far from the ventricle. This suggested that, in the absence of the NSCs, a bulk of neuroblasts uses blood vessels as scaffold for migration. Several recent articles have demonstrated that neuroblasts can use blood vessels as a scaffold to migrate to the cerebral cortex of newborn rats (60), the olfactory bulb of adult rats (61), and damaged brain areas after stroke (62–64).

The fact that all of these cerebral abnormalities are irreversible inborn defects may explain why a large number of hydrocephalic children develop neurologic disorders that are not resolved by surgical treatment.

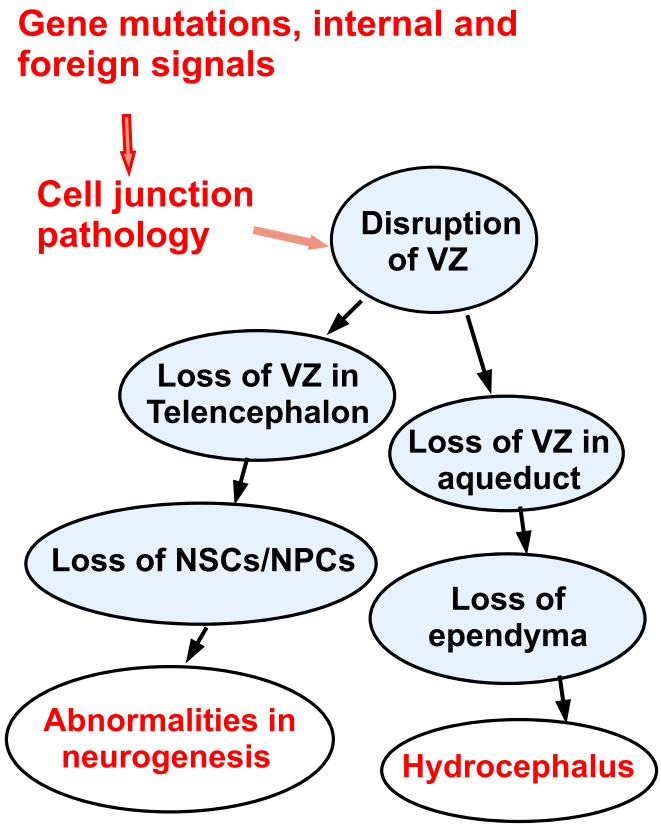

FIGURE 8. Whereas disruption of ventricular zone (VZ) in the aqueduct of Sylvius leads to hydrocephalus, VZ disruption in the telencephalon results in abnormal neurogenesis. Cell junction pathology appears to be a final common pathway of multiple genetic and environmental factors that finally result in the disruption of the VZ. NSCs, neural stem cells; NPCs, neural progenitor cells.

Disrupted NSCs/NPCs Are Shed Into the CSF

In hydrocephalic human fetuses, NSCs/NPCs reach the ventricle at sites of VZ disruption (15, present report) and can be collected from the CSF (15, 65). Furthermore, we found that cells collected from CSF of 2 spontaneously aborted fetuses developed into neurospheres (unpublished finding). In the HTx rat, proliferative βIII-tubulin–positive NPCs from the SVZ reach the ventricle through the sites of VZ disruption and can be collected from the CSF. Nestin-positive NSCs from the VZ also appear to reach the CSF (present report). When processed for the neurosphere assay, cells collected from CSF

FIGURE 7. Disruption of the ventricular zone (VZ) of human hydrocephalic fetuses leads to abnormalities in neurogenesis. (**A**–**A″**) Telencephalon of a human hydrocephalic fetus, 21 gestational weeks (GW) of age, showing periventricular heterotopias (PHs) associated with disruption of the VZ and translocation of cells into the ventricle (**A″**, arrow). (**B, C**) Telencephalon of a human hydrocephalic fetus at 40 GW of age with a large denuded area (**B**, arrows), subependymal rosettes (R), βIII-tubulin (βIII-tub)–positive cells in the perivascular space (**B**, asterisks; **B′, B″**) and PHs formed by βIII-tub–positive cells (**C**, inset). The denuded ventricular surface is covered by a layer of glial fibrillary acidic protein (GFAP)–positive astrocytes (**C**). (**D**) Lateral ventricle of a hydrocephalic human fetus showing VZ disruption (full arrow), subependymal rosettes (R), and SVZ cells translocated into the ventricle (asterisk). Left rectangle, area similar to that of (**F**); broken arrow, denuded region; right rectangle, area similar to that of (**G**). (**E**) Line drawing depicting abnormalities in neurogenesis because of VZ disruption, formation of PHs and translocation of neural progenitor cells into the CSF. (**F, G**) At sites of intact VZ, βIII-tub–positive cells are located in the SVZ (**F**) whereas, at disrupted sites, βIII-tub–positive cells reached the ventricle (**G**). (**H, I**) Cells forming the rosettes having little or no cadherin immunoreactivity (**H**, asterisk) are GFAP positive and have long basal processes (**I**). Scale bars = (**A**–**C**) 300 μm; (**A′**) 120 μm; (**A″**, **F**) 25 μm; (**B′**, **B″**) 40 μm; (**D**) 150 μm; (**G**) 10 μm; (**H, I**) 30 μm.

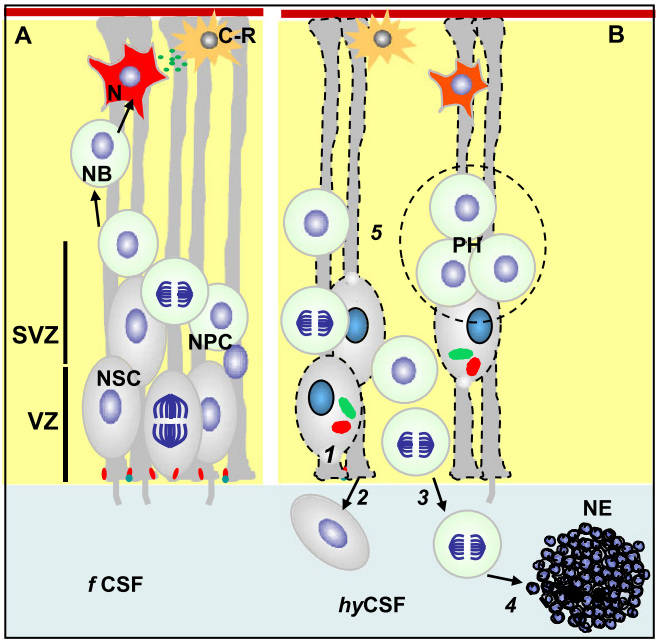

FIGURE 9. (**A**) The ventricular zone (VZ) is formed by neural stem cells (gray, NSCs). The subventricular zone (SVZ) contains the proliferative neural progenitor cells (light green, NPCs), which migrate as neuroblasts (NBs) along radial processes of NSCs and differentiate into neurons (N) that form the cerebral cortex. Cajal-Retzius cell (C-R). VZ cells are joined by adherens and gap junctions (red, blue). Specialized areas of the VZ secrete signal compounds into the fetal cerebrospinal fluid (fCSF). (**B**) Disruption of the VZ because of cell junction pathology of NSCs results in displacement of NSCs [1] and NPCs [2] into the CSF [3]. These cells can be collected from the CSF of hydrocephalic rats and cultured. They develop abnormal neurospheres [4]. The absence of the scaffold provided by NSCs results in arrested neuroblasts that form periventricular heterotopias (PHs) [5].

proliferated and reassembled through adherens junctions to form neurospheres. In view of the different duration of the cell cycle of NSCs and NPCs (66), we suggest that large neurospheres derive from NSCs and small neurospheres from NPCs. This possibility is supported by their distinct immunocytochemical characteristics.

After 2 DIV, the neurospheres started to express an adherens junction pathology and became disrupted, mirroring the features of NSCs in the VZ of live hyHTx rats, as well as that of neurospheres developed from the pallium of hyHTx rats. This finding indicates that a genetic defect and not epigenetic factors, such as increased CSF pressure or changes of CSF composition, underlies the disruption phenomenon. The present findings suggest that NSCs/NPCs collected from the CSF of hydrocephalic patients might be used to investigate cell and molecular alterations underlying the disease.

In summary, the present investigation identifies a new mechanism underlying the abnormal neurogenesis associated with fetal-onset hydrocephalus. Abnormalities of cell junction molecules in NSCs/NPCs are associated with the disruption of the VZ, the formation of PHs, and abnormal translocation of NSCs/NPCs to the fetal CSF. The outcomes of these abnormalities continue to the end of fetal life and most likely continue during postnatal life. These abnormalities might explain some of the neurologic impairments (e.g. epilepsy) of children born with hydrocephalus. They also provide the basis for the use of the neurosphere assay for diagnosis and cell therapy (9, 67). We agree with Del Bigio (68) and Williams et al (69) that better treatment of hydrocephalus and the associated neurologic impairment will come from a better understanding of the biologic basis of the brain abnormalities in hydrocephalus.

ACKNOWLEDGMENT

The authors wish to acknowledge the valuable technical support of Mr Genaro Alvial from Universidad Austral de Chile and Dr Francisco Nualart from Centro de Microscopía Avanzada, Universidad de Concepción, for his support in laser microscopy. Monoclonal antibodies against nestin and BrdU were obtained from the Developmental Studies Hybridoma Bank developed under the auspices of the NICHD and maintained by The University of Iowa, Department of Biological Sciences, Iowa City, Iowa.

REFERENCES

1. Edwards JH. The syndrome of sex-linked hydrocephalus. Arch Dis Child 1961;36:486–93
2. Gilbert JN, Jones KL, Rorke LB, et al. Central nervous system anomalies associated with meningomyelocele, hydrocephalus, and the Arnold-Chiari malformation: Reappraisal of theories regarding the pathogenesis of posterior neural tube closure defects. Neurosurgery 1986;18:559–64
3. Jellinger G. Anatomopathology of nontumoral aqueductal stenosis. J Neurosurg Sci 1986;30:1–16
4. Johnson RT, Johnson KP, Edmonds CJ. Virus-induced hydrocephalus: Development of aqueductal stenosis in hamsters after mumps infection. Science 1967;157:1066–67
5. Boop FA. Posthemorrhagic hydrocephalus of prematurity. In: Cinalli C, Maixner WJ, Sainte-Rose C, eds. *Pediatric Hydrocephalus*. Milan, Italy: Springer-Verlag, 2004:121–31
6. Del Bigio MR. Ependymal cells: Biology and pathology. Acta Neuropathol 2010;119:55–73
7. Jones HC, Klinge PM. Hydrocephalus 2008. 17–20th September, Hannover Germany: A conference report. Cerebrospinal Fluid Res 2008;5:19
8. Carter CS, Vogel T, Zhang Q, et al. Abnormal development of $NG2^+$ $PDGFR\text{-}\alpha^+$ neural progenitor cells leads to neonatal hydrocephalus in a ciliopathy mouse model. Nat Med 2013;18:1797–804
9. Rodríguez EM, Guerra M, Vío K, et al. A cell junction pathology of neural stem cells leads to abnormal neurogenesis and hydrocephalus. Biol Res 2012;45:231–41
10. Rousso DL, Pearson CA, Gaber ZB, et al. Foxp-mediated suppression of N-cadherin regulates neuroepithelial character and progenitor maintenance in the CNS. Neuron 2012;74:314–30
11. Shibasaki T, Tokunaga A, Sakamoto R, et al. PTB deficiency causes the loss of adherens junctions in the dorsal telencephalon and leads to lethal hydrocephalus. Cereb Cortex 2013;23:1824–35
12. Götz M, Huttner WB. The cell biology of neurogenesis. Nat Rev Mol Cell Biol 2005;6:777–88
13. Malatesta P, Appolloni I, Calzolari F. Radial glia and neural stem cells. Cell Tissue Res 2008;331:165–78
14. Merkle FT, Alvarez-Buylla A. Neural stem cells in mammalian development. Curr Opin Cell Biol 2006;18:704–9
15. Domínguez-Pinos MD, Páez P, Jiménez AJ, et al. Ependymal denudation and alterations of the subventricular zone occur in human fetuses with a moderate communicating hydrocephalus. J Neuropathol Exp Neurol 2005;64:595–604
16. Sival DA, Guerra M, den Dunnen WF, et al. Neuroependymal denudation is in progress in full-term human foetal spina bifida aperta. Brain Pathol 2011;21:163–79

17. Jiménez AJ, Tomé M, Páez P, et al. A programmed ependymal denudation precedes congenital hydrocephalus in the hyh mutant mouse. J Neuropathol Exp Neurol 2001;60:1105–19
18. Páez P, Bátiz LF, Roales-Buján R, et al. Patterned neuropathologic events occurring in hyh congenital hydrocephalic mutant mice. J Neuropathol Exp Neurol 2007;66:1082–92
19. Wagner C, Bátiz LF, Rodríguez S, et al. Cellular mechanisms involved in the stenosis and obliteration of the cerebral aqueduct of hyh mutant mice developing congenital hydrocephalus. J Neuropathol Exp Neurol 2003; 62:1019–40
20. Ferland RJ, Bátiz LF, Neal J, et al. Disruption of neural progenitors along the ventricular and subventricular zones in periventricular heterotopia. Hum Mol Genet 2008;18:497–516
21. Oliver C, González C, Alvial G, et al. Disruption of CDH2/N-cadherin-based adherens junctions leads to apoptosis of ependymal cells and denudation of brain ventricular walls. J Neuropathol Exp Neurol 2013;72:846–60
22. Yamamoto H, Maruo T, Majima T, et al. Genetic deletion of afadin causes hydrocephalus by destruction of adherens junctions in radial glial and ependymal cells in the midbrain. PLoS One 2013;8:e80356
23. Chae TH, Kim S, Marz KE, et al. The hyh mutation uncovers roles for Snap in apical protein localization and control of neural cell fate. Nat Genet 2004;36:264–70
24. Ortloff AR, Vío K, Guerra M, et al. Role of the subcommissural organ in the pathogenesis of congenital hydrocephalus in the HTx rat. Cell Tissue Res 2013;352:707–25
25. Sternberger LA, Hardy PH, Cuculis JJ, et al. The unlabeled antibody enzyme method of immunohistochemistry. Preparation and properties of soluble antigen-antibody complex (horseradish peroxidase–antihorseradish peroxidase) and its use in identification of spirochetes. J Histochem Cytochem 1970;18:315–33
26. Rodríguez EM. Fixation of the central nervous system by perfusion of the cerebral ventricles with a threefold aldehyde mixture. Brain Res 1969; 15:395–412
27. Emery JL. Deformity of the aqueduct of Sylvius in children with hydrocephalus and myelomeningocele. Dev Med Child Neurol 1974;16(6 Suppl 32):40–48
28. Koo H, Chi JG. Congenital hydrocephalus-analysis of 49 cases. J Korean Med Sci 1991;6:287–98
29. Peach B. The Arnold-Chiari malformation. Arch Neurol 1965;12:527–35
30. Cinalli G, Spennato P, Del Basso-De Caro ML, et al. Hydrocephalus and Dandy Walker malformation. In: Cinalli C, Maixner WJ, Sainte-Rose C, eds. *Pediatric Hydrocephalus*. Milan, Italy: Springer-Verlag, 2004:259–77
31. Nielsen LA, Maroun LL, Broholm H, et al. Neural tube defects and associated anomalies in a fetal and perinatal autopsy series. APMIS 2006; 114:239–46
32. Jacobsen M. *Developmental neurobiology*. New York, NY: Plenum, 1991
33. Brazel CY, Romanko MJ, Rothstein RP, et al. Roles of the mammalian subventricular zone in brain development. Prog Neurobiol 2003;69:49–69
34. Mori T, Buffo A, Gotz M. The novel roles of glial cells revisited: The contribution of radial glia and astrocytes to neurogenesis. Curr Top Dev Biol 2005;69:67–99
35. Kazanis I. The subependymal zone neurogenic niche: A beating heart in the centre of the brain: How plastic is adult neurogenesis? Opportunities for therapy and questions to be addressed. Brain 2009;132:2909–21
36. Spassky N, Merkle FT, Flames N, et al. Adult ependymal cells are postmitotic and are derived from radial glial cells during embryogenesis. J Neurosci 2005;25:10–18
37. Sarnat HB. Role of human fetal ependyma. Pediatr Neurol 1992;8:163–78
38. Sarnat HB. Regional differentiation of the human fetal ependyma: Immunocytochemical markers. J Neuropathol Exp Neurol 1992;51:58–75
39. Bonfanti L, Peretto P. Radial glial origin of the adult neural stem cells in the subventricular zone. Prog Neurobiol 2007;83:24–36
40. Nojima Y, Enzan H, Hayashi Y, et al. Neuroepithelial and ependymal changes in HTx rats with congenital hydrocephalus: An ultrastructural and immunohistochemical study. Pathol Int 1998;48:115–25
41. Chae TH, Kim S, Marz KE, et al. The hyh mutation uncovers roles for alpha Snap in apical protein localization and control of neural cell fate. Nat Genet 2004;36:264–70
42. Bátiz LF, Páez P, Jiménez AJ, et al. Heterogeneous expression of hydrocephalic phenotype in the hyh mice carrying a point mutation in alpha-SNAP. Neurobiol Dis 2006;23:152–68
43. Klezovitch O, Fernandez TE, Tapscott SJ, et al. Loss of cell polarity causes severe brain dysplasia in Lgl1 knockout mice. Genes Dev 2004;18:559–71
44. Imai F, Akimoto K, Koyama H, et al. Inactivation of aPKClambda results in the loss of adherens junctions in neuroepithelial cells without affecting neurogenesis in mouse neocortex. Development 2006;133:1735–44
45. Ma X, Bao J, Adelstein RS. Loss of cell adhesion causes hydrocephalus in nonmuscle myosin II-B–ablated and mutated mice. Mol Biol Cell 2007;18:2305–12
46. Rasin M, Gazula V, Breunig J, et al. Numb and Numbl are required for maintenance of cadherin-based adhesion and polarity of neural progenitors. Nat Neurosci 2007;10:819–27
47. Kadowaki M, Nakamura S, Machon O, et al. N-cadherin mediates cortical organization in the mouse brain. Dev Biol 2007;304:22–33
48. Shaw RF, Fay AJ, Puthenveedu M, et al. Microtubule plus-end-tracking proteins target gap junctions directly from the cell interior to adherens junctions. Cell 2007;128:547–60
49. Yung YC, Mutoh T, Lin ME, et al. Lysophosphatidic acid signaling may initiate fetal hydrocephalus. Sci Transl Med 2011;3:99ra87
50. Shim JW, Sandlund J, Han CH, et al. VEGF, which is elevated in the CSF of patients with hydrocephalus, causes ventriculomegaly and ependymal changes in rats. Exp Neurol 2013;247:703–9
51. Johanson CE, Duncan JA 3rd, Klinge PM, et al. Multiplicity of cerebrospinal fluid functions: New challenges in health and disease. Cerebrospinal Fluid Res 2008;5:10
52. Vio K, Rodríguez S, Yulis CR, et al. The subcommissural organ of the rat secretes Reissner's fiber glycoproteins and CSF-soluble proteins reaching the internal and external CSF compartments. Cerebrospinal Fluid Res 2008;5:3
53. Mashayekhi F, Draper CE, Bannister CM, et al. Deficient cortical development in the hydrocephalic Texas (H-Tx) rat: A role for CSF. Brain 2002;125(Pt 8):1859–74
54. Miyan JA, Nabiyouni M, Zendah M. Development of the brain: A vital role for cerebrospinal fluid. Can J Physiol Pharmacol 2003;81:317–28
55. Nabiuni M, Rasouli J, Parivar K, et al. In vitro effects of fetal rat cerebrospinal fluid on viability and neuronal differentiation of PC12 cells. Fluids Barriers CNS 2012;9:8
56. Nechiporuk T, Fernández TE, Vasioukhin V. Failure of epithelial tube maintenance causes hydrocephalus and renal cysts in Dlg5$^{-/-}$ mice. Dev Cell 2007;13:338–50
57. Guerrini R, Barba C. Malformations of cortical development and aberrant cortical networks: Epileptogenesis and functional organization. J Clin Neurophysiol 2010;27:372–79
58. Sato O, Yamguchi T, Kittaka M, et al. Hydrocephalus and epilepsy. Childs Nerv Syst 2001;17:76–86
59. Vinchon M, Rekate H, Kulkarni AV. Pediatric hydrocephalus outcomes: A review. Fluids Barriers CNS 2012;9:18
60. Le Magueresse C, Alfonso J, Bark C, et al. Subventricular zone-derived neuroblasts use vasculature as a scaffold to migrate radially to the cortex in neonatal mice. Cereb Cortex 2012;22:2285–96
61. Bovetti S, Hsieh YC, Bovolin P, et al. Blood vessels form a scaffold for neuroblast migration in the adult olfactory bulb. J Neurosci 2007;27: 5976–80
62. Cayre M, Canoll P, Goldman JE. Cell migration in the normal and pathological postnatal mammalian brain. Prog Neurobiol 2009;88:41–63
63. Thored P, Wood J, Arvidsson A, et al. Long-term neuroblast migration along blood vessels in an area with transient angiogenesis and increased vascularization after stroke. Stroke 2007;38:3032–39
64. Yamashita T, Ninomiya M, Hernández-Acosta P, et al. Subventricular zone–derived neuroblasts migrate and differentiate into mature neurons in the post-stroke adult striatum. J Neurosci 2006;26:6627–36
65. Krueger RC, Wu H, Zandian M, et al. Neural progenitors populate the cerebrospinal fluid of preterm patients with hydrocephalus. J Pediatr 2006; 148:337–40
66. Ponti G, Obernier K, Guinto C, et al. Cell cycle and lineage progression of neural progenitors in the ventricular-subventricular zones of adult mice. PNAS 2013;110:1045–54
67. Guerra M. Neural stem cells: Are they the hope of a better life for patients with fetal-onset hydrocephalus? Fluids Barriers CNS 2014;11:7
68. Del Bigio MR. Pathophysiologic consequences of hydrocephalus. Neurosurg Clin N Am 2001;12:639–49
69. Williams MA, McAllister JP, Walker ML, et al. Priorities for hydrocephalus research: Report from a National Institutes of Health–sponsored workshop. J Neurosurg 2007;107:345–57